Sensory neuron population expansion enhances odour tracking without sensitising projection neurons

Suguru Takagi[1,11,*], Gizem Sancer[2,12], Liliane Abuin[1,12], S. David Stupski[3,12], J. Roman Arguello[1,4,5], Lucia L. Prieto-Godino[1,6], David L. Stern[7], Steeve Cruchet[1], Raquel Álvarez-Ocaña[1], Carl F. R. Wienecke[8,9], Floris van Breugel[3], James M. Jeanne[2], Thomas O. Auer[1,10,11,13,*] and Richard Benton[1,13,*]

[1]Center for Integrative Genomics, Faculty of Biology and Medicine, University of Lausanne, Lausanne, Switzerland

[2]Department of Neuroscience, Yale University, New Haven, Connecticut, USA

[3]Department of Mechanical Engineering, University of Nevada, Reno, Nevada, USA

[4]Department of Ecology and Evolution, Faculty of Biology and Medicine, University of Lausanne, Lausanne, Switzerland

[5]Swiss Institute of Bioinformatics, Lausanne, Switzerland

[6]The Francis Crick Institute, London, UK

[7]Janelia Research Campus of the Howard Hughes Medical Institute, Ashburn, Virginia, USA

[8]Department of Neurobiology, Stanford University, Stanford, California, USA

[9]Present address: Department of Neurobiology, Harvard Medical School, Cambridge, Massachusetts, USA

[10]Present address: Department of Biology, University of Fribourg, Fribourg, Switzerland

[11]These authors contributed equally to this work
[12]These authors contributed equally to this work
[13]Joint senior authors

[*]Corresponding authors:
Suguru.Takagi@unil.ch
Thomas.Auer@unifr.ch
Richard.Benton@unil.ch

Abstract

From the star-nosed mole's eponymous mechanosensory organ to the platypus' electroreceptive bill, the expansion of sensory neuron populations detecting important environmental cues is a widespread evolutionary phenomenon[1-6]. How such neuron increases contribute to improved sensory detection and behaviour remain largely unexplained. Here we address this question through comparative analysis of olfactory pathways in *Drosophila melanogaster* and its close relative *Drosophila sechellia*, which feeds and breeds exclusively on *Morinda citrifolia* noni fruit[7-9]. We show that *D. sechellia* displays species-specific, large expansions in select, noni-detecting olfactory sensory neuron (OSN) populations, and that this trait has a multigenic basis. In noni odour plume-tracking assays, *D. sechellia* exhibits enhanced performance compared to *D. melanogaster*. Through activation and inhibition of defined proportions of one noni-sensing OSN population, we establish that higher number of OSNs contributes to stronger, more persistent behaviour. OSN population expansions are accompanied by an increase in synaptic connections with their projection neuron (PN) partners that transmit information to higher brain centres. Quantification of odour-evoked activity of partner OSNs and PNs reveals that, surprisingly, larger numbers of OSNs does not lead to greater PN sensitivity or response reliability. Rather, these pathways – but not those with conserved OSN numbers – exhibit reduced adaptation of PN activity upon odour stimulation, likely through weakened lateral inhibition. Our work reveals an unexpected functional impact of sensory neuron expansions that can synergise with peripheral receptor tuning changes to explain ecologically-relevant, species-specific behaviour.

Introduction

Brains display incredible diversity in neuron number between animal species[10-12]. Increases in the number of neurons during evolution occur not only through the emergence of new cell types but also through expansion of pre-existing neuronal populations[13,14]. Of the latter phenomenon, some of the most spectacular examples are found in sensory systems: the snout of the star-nosed mole (*Condylura cristata*) has ~25,000 mechanosensory organs, several fold more than other mole species[1]. Male (but not female) moths can have tens of thousands of neurons detecting female pheromones, representing the large majority of sensory neurons in their antennae[15]. A higher number of sensory neurons is generally assumed to underlie sensitisation to the perceived cues[3-6]. Surprisingly, however, it remains largely untested if and how such neuronal expansions impact sensory processing and behaviour.

The drosophilid olfactory system is an excellent model to address these questions[16,17]. The antenna, the main olfactory organ, houses ~1000 olfactory sensory neurons (OSNs) that, in *Drosophila melanogaster*, have been classified into ~50 types based on their expression of one (or occasionally more) Odorant receptors (Ors) or Ionotropic receptors (Irs)[17-19]. The size of individual OSN populations (ranging from ~10-65 neurons) is stereotyped across individuals, reflecting their genetically hard-wired, developmental programmes[20,21]. By contrast, comparisons of homologous OSN types in ecologically-distinct drosophilid species have identified several examples of expansions in OSN populations. Notably, *Drosophila sechellia*, an endemic of the Seychelles that

specialises on *Morinda citrifolia* "noni" fruit[7-9], has an approximately three-fold increase in the neuron populations expressing Or22a, Or85b and Ir75b compared to both *D. melanogaster* and a closer relative, *Drosophila simulans*[22-25] (**Fig. 1a**). All three of these neuron classes are required for long- and/or short-range odour-guided behaviours[23,26] and two of these (Or22a and Ir75b) also display increased sensitivity to noni odours through mutations in the corresponding *D. sechellia* receptor genes[22-24]. Together, these observations have led to a long-held assumption that these OSN population expansions are important for *D. sechellia*, but this has never been tested.

Results

Selective large increases in Or22a and Or85b populations in *D. sechellia*

The increase in Or22a and Or85b OSN numbers in *D. sechellia* reflects the housing of these cells in a common sensory hair, the antennal basiconic 3 (ab3) sensillum (**Fig. 1b, Extended Data Fig. 1a,b**). To determine how unique this increase is within the antenna, we compared the number of the other ~20 morphologically-diverse, olfactory sensillar classes – which each house distinct, stereotyped combinations of 1-4 OSN types – in *D. sechellia*, *D. melanogaster* and *D. simulans* through RNA FISH of a diagnostic *Or* per sensillum (combined with published data on *Ir* neurons[22]) (**Fig. 1c**). We observed several differences in sensillar number between these species, including reductions in ab5, ab8 and ai1 in *D. sechellia*, but only ab3, as well as ac3I that house Ir75b neurons, showed a more than two-fold increase (~50 more ab3, 2.6-fold increase; ~15 more ac3I, 3.7-fold increase) in *D. sechellia*. The total number of antennal sensilla is, however, similar across species (**Fig. 1c**).

OSN population expansion is a complex genetic trait

We next investigated the mechanism underlying the ab3 OSN population expansion in *D. sechellia*. The number of ab3 sensilla was not different when these flies were grown in the presence or absence of noni substrate (**Extended Data Fig. 1c**), arguing against an environmental influence. We first asked whether the ab3 increase could be explained by simple transformation of sensillar fate. Previous electrophysiological analyses reported loss of ab2 sensilla in *D. sechellia*, which was interpreted as a potential trade-off for the ab3 expansion[24,27]. However, we readily detected ab2 sensilla histologically in this species (**Fig. 1c, Extended Data Fig. 1d**), countering this possibility. Moreover, from an antennal developmental fate map in *D. melanogaster*[28], we did not observe any obvious spatial relationship between the sensory organ precursors for sensillar classes that display increases or decreases in *D. sechellia* to support a hypothesis of a simple fate switch, although both expanded populations (ab3 and ac3I) originate from peripheral regions of the map (**Extended Data Fig. 1e**).

We therefore reasoned that genetic changes specifically affecting the development of the ab3 lineage might be involved. We first tested for the existence of species-specific divergence in *cis*-regulation at the receptor loci. Using mutants for both *Or22a/(b)* and *Or85b* in *D. simulans* and *D. sechellia*[23], we analysed receptor expression in interspecific hybrids and reciprocal hemizygotes (lacking transcripts from one or the other receptor allele) (**Fig. 1d, Extended Data Fig. 1f**).

In all hybrid allelic combinations (except those lacking both alleles) we observed a similar number of Or22a and Or85b OSNs, arguing against a substantial contribution of *cis*-regulatory evolution at these loci to the expansion of receptor neuronal expression.

As little is known about the developmental programme of ab3 specification, we used an unbiased, whole-genome, quantitative trait locus (QTL) mapping strategy to characterise the genetic basis of the expansion in *D. sechellia*. For high-throughput quantification of ab3 numbers, we generated fluorescent reporters of Or85b neurons in *D. sechellia* and *D. simulans* (**Extended Data Fig. 2a,b**). Interspecific F1 hybrids displayed an intermediate number of Or85b neurons to the parental strains (**Fig. 1e**). We phenotyped >600 F2 individuals (backcrossed to either *D. sechellia* or *D. simulans*) (**Fig. 1e**), which were then genotyped using multiplexed shotgun sequencing[29]. The resulting QTL map (**Fig. 1f**) identified two genomic regions linked to variation in Or85b neuron number located on chromosomes 3 and X; these explain a cell number difference of about ~12 and ~7 neurons, respectively, between *D. sechellia* and *D. simulans* (**Fig. 1g**). No significant epistasis was detected between these genomic regions (**Methods**) and the relatively low effect size (21.0% and 12.3%, respectively) is consistent with a model in which more than two loci contribute to the species difference in Or85b neuron number. Consistent with the QTL map, introgression of fragments of the *D. sechellia* genomic region spanning the chromosome 3 peak into a *D. simulans* background led to an increased number of Or85b neurons (**Extended Data Fig. 2c,d**). However, the phenotypic effect was lost with smaller introgressed regions, indicating that multiple loci influencing Or85b neuron number are located within this QTL region (**Extended Data Fig. 2d**).

In a separate QTL mapping of the genetic basis for the increase in ac3I (Ir75b) neurons in *D. sechellia*[22] (**Fig. 1c**), we also observed a complex genetic architecture of this interspecific difference, with no evidence for shared loci with the ab3 sensilla expansion (**Extended Data Fig. 2j,k)**. Thus, in contrast to the evolution of sensory specificity of olfactory pathways – where only one or a few amino acid substitutions in a single receptor can have a phenotypic impact[22,23,26], with some evidence for "hotspot" sites in different receptors[30] – species differences in the number of OSN types have arisen from distinct evolutionary trajectories involving changes at multiple loci.

Or22a is required for *D. sechellia* to track host odour

We next investigated if and how increased OSN population size impacts odour-tracking behaviour. Previously, we showed that both Or22a and Or85b pathways are essential for long-range attraction to noni in a wind tunnel[23]. To analyse the behavioural responses of individual animals to odours with greater resolution, we developed a tethered fly assay[31] with a timed odour-delivery system (**Fig. 2a**). By measuring the beating amplitude of both wings while presenting a lateralised odour stimulus, we could quantify attractive responses to individual odours, as reflected in an animal's attempt to turn toward the stimulus source, leading to a positive delta wing beat amplitude (*ΔWBA*) (see **Methods**). We first tested responses of wild-type flies to consecutive short pulses of noni odours, which mimic stimulus dynamics in a plume. As expected, multiple strains of *D. sechellia* displayed attractive responses that persisted through most or all of the series of odour pulses, while *D. melanogaster* strains displayed much more variable degrees of attraction

(**Fig. 2b, Extended Data Fig. 3a**). The persistent attraction in *D. sechellia* was specific to noni odour and could not be observed using apple cider vinegar (**Extended Data Fig. 3b**).

To assess the contribution of distinct olfactory pathways to noni attraction, we tested *D. sechellia* mutants for *Or22a*, *Or85c/b*, *Ir75b* and, as a control, *Or35a*, whose OSN population is also enlarged (as it is paired with Ir75b neurons in ac3I) but is dispensable for noni attraction[23]. Loss of *Or22a* abolished attraction of flies towards noni, while *Or85c/b* and *Ir75b* mutants retained some, albeit transient, turning towards this stimulus. Flies lacking *Or35a* behaved comparably to wild-type strains (**Fig. 2c**). These results point to Or22a as an important (albeit not the sole) olfactory receptor required for *D. sechellia* to respond behaviourally to noni odour.

To better understand the nature of *D. sechellia* plume-tracking in a more natural setting, we used a wind-tunnel assay combined with 3D animal tracking[32] to record trajectories of freely-flying wild-type *D. melanogaster* and *D. sechellia*, as they navigated to the source of a noni juice odour plume (**Fig. 2d, Extended Data Fig. 4a,b**). Wild-type *D. sechellia* exhibited similar cast and surge dynamics as *D. melanogaster*[33] (**Fig. 2d**). However, we observed that *D. sechellia* maintained flight paths closer to the plume centreline (**Fig. 2d-f**), a difference that was particularly evident close (<20 cm) to the plume source (**Fig. 2d-f**). Consistent with the phenotype observed in the tethered-fly assay, *D. sechellia Or22a* mutants lacked strong plume-tracking responses (**Fig. 2d-f**), while not exhibiting obvious impairment in flight performance (**Extended Data Fig. 4c**). To extend analysis of these observations we quantified the distribution of flies within a 3 cm radius of the estimated odour plume centreline in the downwind and upwind halves of the wind tunnel (**Fig. 2e,g**). In the downwind half, wild-type *D. sechellia* and *D. melanogaster* had comparable course direction distributions (**Fig. 2g**). By contrast, in the upwind half, *D. sechellia* maintained a tighter upwind course distribution suggesting they were more likely to be in an upwind surging state compared to *D. melanogaster* as they approach the odorant source (**Fig. 2g**). *D. sechellia Or22a* mutants did not appear to be strongly oriented into the wind, notably in the downwind half, further indicating the importance of this olfactory pathway in stereotypical plume-tracking behaviours (**Fig. 2g**).

D. sechellia's increase in OSN number is important for persistent odour-tracking behaviour

To investigate the importance of Or22a neuron number for odour-tracking behaviour we expressed CsChrimson in Or22a neurons in *D. melanogaster* and *D. sechellia* to enable specific stimulation of this pathway with red light. This optogenetic approach had two advantages: first, it allowed us to calibrate light intensity to ensure equivalent Or22a OSN activation between species; second, because only Or22a neurons are activated by light, we could eliminate sensory contributions from other olfactory pathways that have overlapping odour tuning profiles to Or22a.

We first confirmed light-evoked spiking in Or22a neurons in *D. melanogaster* and *D. sechellia* and determined the light intensity evoking equivalent spike rates (**Fig. 3a**). We then performed lateralised optogenetic activation[34] of Or22a OSNs in the tethered fly assay, mimicking lateralised odour input by focussing the light beam on one antenna (**Fig. 3a, Extended Data Fig. 5a**). Pulsed optogenetic activation of *D. sechellia* Or22a OSNs induced attractive behaviour with a similar

magnitude and dynamics as pulsed odour stimuli (**Fig. 3b**), demonstrating the sufficiency of this single olfactory pathway for evoking behaviour. Notably, the attractive behaviour was more persistent over the series of light pulses in *D. sechellia* than in *D. melanogaster* (**Fig. 3a, Extended Data Fig. 5b-d**), consistent with a hypothesis that a higher number of Or22a OSNs supports enduring behavioural attraction to a repeated stimulus.

To explicitly test this possibility, we generated genetic tools to reproducibly manipulate the number of active Or22a OSNs in *D. sechellia*, using the SPARC technology developed in *D. melanogaster*[35] (**Extended Data Fig. 6a**). Combining a *SPARC2-D-CsChrimson* transgene with *Or22a-Gal4* allowed us to optogenetically stimulate ~50% of these neurons (**Fig. 3c, Extended Data Fig. 6b**). Although we confirmed light-evoked Or22a neuron spiking in these animals, they did not display attractive behaviour towards the light stimulus, in contrast to similar stimulation of all Or22a OSNs (**Fig. 3c, Extended Data Fig. 6c**). This result implies that the number of active OSNs is critical to induce attraction in *D. sechellia*.

Optogenetic activation of Or22a neurons only partially mimics differences between species because it does not offer the opportunity for any possible plasticity in circuit properties that are commensurate with differences in OSN number (as described below). We therefore took a complementary approach, through neuronal silencing, using a *SPARC2-D-Tetanus Toxin* (*TNT*) transgene. With this tool we could silence on average ~50% of Or22a OSNs (**Fig. 3d**) – likely from mid/late-pupal development (when the *Or22a* promoter is activated[36]) – without directly inhibiting other peripheral or central neurons (**Extended Data Fig. 6d**). Importantly, when tested in our tethered flight assay, these flies showed weaker and more transient attraction towards noni odour, contrasting with the persistent noni attraction of control animals (**Fig. 3d**)**.** Together these results support the hypothesis that the increased Or22a OSN number observed in *D. sechellia* is essential for strong and sustained attractive olfactory behaviour.

OSN population expansions lead to increased pooling on cognate projection neurons

To better understand how increased OSN number might enhance odour-guided behaviour, we first characterized the anatomical properties of the circuitry. The axons of OSNs expressing the same receptor converge onto a common glomerulus within the antennal lobe in the brain[37] (**Fig. 4a**). Here, they form cholinergic synapses on mostly uniglomerular projection neurons (PNs) – which transmit sensory signals to higher olfactory centres – as well as on broadly-innervating local interneurons (LNs) and a small proportion on other OSNs[37,38]. To visualise PNs in *D. sechellia*, we generated specific driver transgenes in this species using constructs previously-characterised in *D. melanogaster*[39,40]: *VT033006-Gal4*, which drives expression in many uniglomerular PN types and *VT033008-Gal4* which has sparser PN expression (**Fig. 4b**). Using these drivers to express photoactivable-GFP in PNs, we performed spatially-limited photoactivation of the DM2 and VM5d glomeruli – which receive input from Or22a and Or85b OSNs, respectively (**Fig. 4a**) – to visualise the partner PNs. We confirmed that DM2 is innervated by 2 PNs in both *D. melanogaster* and *D. sechellia*[23] and further found that VM5d also has a conserved number of PNs (on average 4) in these species (**Fig. 4c**). Together with data that the Ir75b glomerulus, DL2d, has the same number of PNs in *D. melanogaster*, *D. simulans* and *D. sechellia*[22,41], these

observations indicate that *D. sechellia*'s OSN population expansions are not accompanied by increases in PN partners.

Next, we expressed a post-synaptic marker, the GFP-tagged Dα7 acetylcholine receptor subunit, in PNs[38,42,43] in *D. melanogaster* and *D. sechellia* (**Fig. 4d**). Quantification of glomerular volume as visualised with this reporter confirmed previous observations, using OSN markers[22-25,41], that the DM2 and VM5d glomeruli, but not a control glomerulus (DM6), are specifically increased in *D. sechellia* compared to *D. melanogaster* (**Fig. 4e**). Given the constancy in PN number (**Fig. 4c**), this observation implied that PN dendrites must exhibit anatomical differences to occupy a larger volume. We examined this possibility through visualisation of single VM5d PNs by dye-labelling (in the course of electrophysiology experiments described below). Reconstruction of dendrite morphologies revealed that *D. sechellia* VM5d PNs have increased dendritic surface area and volume compared to the homologous neurons in *D. melanogaster* (**Fig. 4f**).

Finally, we quantified post-synaptic puncta of Dα7:GFP to estimate the number of excitatory OSN-PN connections in these glomeruli. Both DM2 and VM5d, but not DM6, displayed more puncta in *D. sechellia* than in *D. melanogaster* (**Fig. 4g**). Although quantifications of fluorescent puncta are likely to substantially underestimate the number of synapses detectable by electron microscopy[37,38], this reporter should still reflect the relative difference between species. Together these data suggest that an increase in OSN numbers leads to larger glomerular volumes, increased dendritic arborisation in partner PNs and overall more synaptic connections between OSNs and PNs.

OSN number increases do not lead to sensitisation of PN responses

To investigate the physiological significance of these OSN-PN circuit changes, we generated genetic reagents to visualise and thereby perform targeted electrophysiological recordings from specific PNs. We focused on VM5d PNs due to the availability of an enhancer-Gal4 transgene for sparse genetic labelling of this cell type[44]. Moreover, the partner Or85b OSNs' sensitivities to the best-known agonist, *2*-heptanone, are indistinguishable between species[23], enabling specific assessment of the impact of OSN population expansion on PN responses. Through whole-cell patch clamp recordings from VM5d PNs in *D. melanogaster* and *D. sechellia* (**Fig. 5a**), we first observed that the input resistance of these cells was ~2-fold lower in *D. sechellia* (**Fig. 5b**), consistent with their larger dendritic surface area and volume (**Fig. 4f**). The resting membrane potential (**Fig. 5c**) and spontaneous activity (**Fig. 5d**) of these PNs were, however, unchanged between species. Surprisingly, VM5d PNs displayed no obvious increase in odour sensitivity in *D. sechellia* (**Fig. 5e, Extended Data Fig. 7a**); if anything, the peak spiking rate (within the first 50 ms after PN response onset) tended to be higher in *D. melanogaster*. However, we observed that the PN firing during the odour stimulus displayed a starker decay in *D. melanogaster* than *D. sechellia* (**Fig. 5f, Extended Data Fig. 7b**). These data support a model in which increased synaptic input by more OSNs in *D. sechellia* is compensated by decreased PN input resistance precluding the sensitisation of responses in this cell type. Instead, OSN increases might impact the temporal dynamics of PN responses (explored further below).

To substantiate and extend these observations, we expressed GCaMP6f broadly in OSNs or PNs and measured odour-evoked responses in specific

glomeruli using two-photon calcium imaging. When measuring calcium responses to a short pulse of *2*-heptanone in Or85b OSN axon termini in the VM5d glomerulus, we observed, as expected[23], no sensitivity differences (**Fig. 5g, Extended Data Fig. 8a**). VM5d PNs also displayed no obvious increase in odour sensitivity in *D. sechellia* (**Fig. 5g, Extended Data Fig. 8b**), consistent with our patch clamp recordings (**Fig. 5e**). Next, we investigated Or22a OSNs and DM2 PNs after stimulation with the noni odour methyl hexanoate[24]. In this olfactory pathway, *D. sechellia* OSNs displayed responses at odour concentrations approximately two orders of magnitude lower than in *D. melanogaster* (**Fig. 5h, Extended Data Fig. 8c**), concordant with previous electrophysiological analyses[23,24,27]. *D. sechellia* DM2 PNs displayed a similar degree of heightened sensitivity compared to those in *D. melanogaster*, supporting that an increased Or22a OSN number does not lead to further sensitisation of these PNs (**Fig. 5h, Extended Data Fig. 8d**). To test the sufficiency of differences in receptor properties[23] to explain PN activity differences, we expressed *D. melanogaster* or *D. sechellia* Or22a in *D. melanogaster* Or22a neurons lacking the endogenous receptors. This manipulation conferred a species-specific odour response profile to these OSNs[23]. Measurement of responses to methyl hexanoate in DM2 PNs revealed higher sensitivity in animals expressing *D. sechellia* Or22a compared to those expressing *D. melanogaster* Or22a (**Extended Data Fig. 8e**); notably, this difference was similar in magnitude to the endogenous sensitivity differences of *D. sechellia* and *D. melanogaster* DM2 PNs. Together, the analyses of Or85b and Or22a pathways indicate that a larger OSN population does not contribute to enhanced PN sensitisation.

OSN number increases do not lead to increased reliability of PN responses

Pooling of inputs on interneurons has also been suggested to reduce the noise in central sensory representations, since spontaneous activity of each OSN is uncorrelated and becomes averaged out as OSN activities are summated at PNs[45-47]. This phenomenon should reduce the variability of PN response magnitude across multiple odour presentations. We therefore examined whether increased OSN number plays a role in reducing trial-to-trial variability in PN responses by comparing odour responses, and their variation, in VM5d PNs to eight trials of *2*-heptanone stimulation. These experiments did not reveal any differences in PN response reliability between *D. melanogaster* and *D. sechellia* (**Extended Data Fig. 9**). Consistent with this calcium imaging analyses, the lack of a significant difference in VM5d PN spontaneous spiking frequency between species (**Fig. 5d**) also argues that increased sensory pooling in *D. sechellia* does not substantially reduce noise in this circuitry.

Pathways with increased OSN number display reduced decay magnitude of PN responses

Most natural odours exist as turbulent plumes, which stimulate OSNs with complex, pulsatile temporal dynamics[33]. To test if odour temporal dynamics in these olfactory pathways are influenced by OSN number, we repeated the calcium imaging experiments using ten consecutive, short pulses of odour. Or85b OSNs displayed a plateaued response to pulses of *2*-heptanone in both *D. melanogaster* and *D. sechellia*, albeit with a slight decay over time in the latter species (**Fig. 5i**). *D.*

melanogaster VM5d PNs showed decreasing responses following repeated exposure to short pulses, presumably reflecting adaptation, as observed in multiple PN types[48]. By contrast, VM5d PNs in *D. sechellia* displayed responses of similar magnitude throughout the series of odour pulses (**Fig. 5j**). This species difference in PN responses was also seen with long-lasting odour stimulation (**Extended Data Fig. 10**) and is consistent with a smaller difference between spiking frequencies at the start and end of odour stimulation in *D. sechellia* VM5d PNs measured by electrophysiological recordings (**Fig. 5f and Extended Data Figure 7b**). Imaging the responses of Or22a OSN partner PNs in DM2 to pulsed odour stimuli (using concentrations of methyl hexanoate that evoked similar activity levels between the species (**Fig. 5h**)) revealed a similar result: *D. melanogaster* DM2 PN responses decreased over time while *D. sechellia* DM2 PNs responses were unchanged in magnitude (**Fig. 5k**). However, for two olfactory pathways where the numbers of cognate OSNs are not increased in *D. sechellia* (Or59b (DM4) and Or92a (VA2) (**Fig. 1c**)), the PNs in both species displayed decreasing responses over the course of stimulations (**Fig. 5l,m, Extended Data Fig. 11**). Together, our data indicate that OSN number increases in *D. sechellia*'s noni-sensing pathways might result, directly or indirectly, in reduced decay magnitude of PN responses to dynamic or long-lasting odour stimuli.

Species-specific PN response properties are due, at least in part, to differences in lateral inhibition

More sustained PN responses in *D. sechellia* could be due to species differences in several aspects of glomerular processing, involving OSNs, PNs and/or LNs. We examined this phenomenon through calcium imaging in VM5d PNs before and after pharmacological inhibition of different synaptic components. Blockage of inhibitory neurotransmission – which is principally mediated by LNs acting broadly across glomeruli[49-51] – decreased adaptation in *D. melanogaster* VM5d PNs, as expected. This effect was predominantly due to inhibition of $GABA_B$ rather than $GABA_A$/GluCl receptors (**Extended Data Fig. 12a,b**). By contrast, inhibitory neurotransmitter receptor blockage did not lead to changes in temporal dynamics of responses in *D. sechellia* (**Fig. 6a and Extended Data Fig. 12a,b**). These observations suggest that differences in the strength of inhibition between species contribute to differences in PN decay magnitude (see Discussion). We note that *D. sechellia* PNs displayed apparent decreases in odour response magnitude (as measured by $\Delta F/F$) upon pharmacological treatment (**Fig. 6a**), but this effect is most likely due to elevated baseline activity (F_0) in this species (**Extended Data Fig. 12c**).

We next pharmacologically impaired cholinergic neurotransmission to diminish excitatory connections of OSNs, which include OSN-PN and likely also OSN-LN synapses[37,48,52,53]. As expected, strong blockage essentially abolished odour-evoked PN responses (data not shown). More informatively, weak blockage led to enhanced decay in the VM5d PN responses of *D. sechellia* (**Fig. 6b**), as seen in untreated *D. melanogaster* (**Fig. 6b**). These observations suggest that excitatory neurotransmission from OSNs to PN and/or LNs also contributes to the temporal dynamics of PN responses. Consistent with this possibility, halving the number of OSN inputs in *D. sechellia* through removal of one antenna (OSN axons project to antennal lobes in both brain hemispheres[37]) enhanced the decay of this species' VM5d PN responses (**Fig. 6c**). These data support the hypothesis that OSN number increase in *D. sechellia* modulates PN response dynamics.

Discussion

Amongst the many ways in which animal brains have diverged during evolution, species-specific increases in the number of a particular neuron type are one of the most common. The genetic basis and physiological and behavioural consequences of such apparently simple changes have, however, remained largely unexamined. Here we have exploited an ecologically and phylogenetically well-defined model clade of drosophilids to study this phenomenon. We provide evidence that expansion of host fruit-detecting OSN populations in *D. sechellia* is a complex trait, involving contributions of multiple loci. Surprisingly, a larger number of OSNs does not result in sensitisation of partner PNs nor in increased reliability of their responses. Rather we observed more sustained responses of PNs upon repetitive or long-lasting odour stimulation. While OSN number alone can influence the strength and persistence of odour-tracking behaviour, this species-specific cellular trait is likely to synergise with increases in peripheral sensory sensitivity conferred by changes in olfactory receptor tuning properties[22-24] to enable long-distance localisation of the host fruit of this species (**Fig. 6d**).

One important open question is how OSN population increases affect circuit properties and behaviour. For one experimentally-accessible glomerulus, VM5d, we observed that PNs (which are unchanged in number between species) have a larger surface area and form more synapses with OSNs but show lower dendritic input resistance in *D. sechellia*. This anatomical and physiological compensation results in the voltage responses of PNs being very similar between species despite the increased OSN input in *D. sechellia*. Such compensation might reflect in-built plasticity in glomerular microcircuitry. Indeed, *D. melanogaster* shows intra-species difference in OSN number across glomeruli[18] and the number of OSNs correlates with synapse number (**Extended Data Fig. 13a**[37]). Moreover, a previous study in *D. melanogaster* characterised the consequence of (random) differences in PN numbers in a glomerulus (DM6): in glomeruli with fewer PNs (i.e. greater sensory convergence per neuron), individual PNs had larger dendrites, formed more synapses with OSNs, and exhibited lower input resistance[54], analogous to our observations in *D. sechellia* VM5d.

Species-specific physiological responses to prolonged or repetitive odour stimuli likely involves multiple neuron classes. In *D. melanogaster*, adaptation of PNs to long odour stimuli occurs through lateral inhibition by GABAergic LNs[49,55], as we confirmed here. However, such inhibition appears to be weaker in *D. sechellia* in pathways with more OSNs. Given the conserved total number of antennal OSNs between species, more OSNs in one pathway could lead to stronger inhibitory neurotransmission from the correspondingly larger glomerulus to other unchanged or smaller glomeruli. Critically, this could result in net weaker lateral inhibition from these glomeruli onto the expanded glomerulus, as seen in *D. sechellia*. We cannot exclude that LNs display species-specific innervations or connectivity, but testing this idea will require genetic drivers to visualise and manipulate subsets of this highly diverse neuron type[56]. Finally, we note that it is also possible that differences exist in the intrinsic physiology of PNs due to, for example, differential expression of ion channels between species. Such differences – potentially unrelated to changes in OSN number – might be revealed by mining comparative transcriptomic datasets for these drosophilids[57].

Regardless of the precise mechanism, could more sustained PN responses convert to behavioural persistence? The main post-synaptic partners of PNs are lateral horn neurons and Kenyon cells, of which the latter (at least) have a high input threshold[58] for sparse coding. Assuming the threshold of these neurons is commensurate with maximum PN firing rate (which is higher in *D. melanogaster*), the relaxed decay in PN activity in *D. sechellia* might elongate downstream responses to persistent odours, which could drive valence-specific behaviours[59]. Sensory habituation is advantageous for the brain to avoid information overload by attenuating constant or repetitive inputs and is a general feature across sensory modalities[60]. However, this phenomenon might be disadvantageous when navigating through sensory cues for a long period of time, for example, during olfactory plume-tracking. The reduced adaptation selectively in PNs in the expanded sensory pathways in *D. sechellia* that detect pertinent host odours provides an elegant resolution to this conflict in sensory processing, leaving conserved molecular effectors mediating synaptic neurotransmission and adaptation in other olfactory pathways intact.

Beyond *D. sechellia*, selective increases in ab3 neuron numbers have been reported in at least two other drosophilid species, which are likely to represent independent evolutionary events[4,61] (**Extended Data Fig. 13b**). Furthermore, Or22a neurons display diversity in their odour specificity across drosophilids[61,62]. These observations suggest that this sensory pathway is an evolutionary "hotspot" where changes in receptor tuning and OSN population size collectively impact sensory processing, perhaps reflecting the potent behavioural influence of this pathway, as we have found in *D. sechellia*. More generally, given our demonstration of the important effect of OSN population size on host odour processing in *D. sechellia*, examination of how cell number increases modify circuit properties in other sensory systems, brain regions and species seems warranted.

Acknowledgements

We thank Hokto Kazama, Johannes Larsch, Silke Sachse and members of the Benton laboratory for discussions and/or comments on the manuscript. We are grateful to Yoshi Aso, John Carlson, Sophie Caron, Tom Clandinin, Heather Dionne, Lukas Neukomm, Gerald Rubin, Stephan Sigrist, the Bloomington *Drosophila* Stock Center (NIH P40OD018537) and the Developmental Studies Hybridoma Bank (NICHD of the NIH, University of Iowa) for reagents. We also thank Jesse Isaacman-Beck for construct design, Anabela Rebelo Pimentel for her assistance with embryo alignments for microinjections, and the Lausanne Genomic Technologies Facility for sequencing. S.T. was supported by a Marie Skłodowska-Curie Actions Individual Fellowship (836783), an EMBO Long-Term Fellowship (ALTF 454-2019) and a Japanese Society for the Promotion of Science (JSPS) Overseas Research Fellowship (202360258). Research in J.R.A.'s lab was supported by the Swiss National Science Foundation (PP00P3_176956 and 310030_201188). C.F.R.W. was support by a National Institutes of Health grant (R01EY022638) to Tom Clandinin. F.v.B.'s laboratory was supported by the Air Force Office of Scientific Research (FA9550-21-0122). G.S. and J.M.J. were supported by NIH grants R01 DC018570 and R01 NS116584, the Richard and Susan Smith Family Award for Excellence in Biomedical Research, the Klingenstein-Simons Fellowship Award in Neuroscience, and an innovative research award from the Kavli Institute for Neuroscience at Yale University to J.M.J.

T.O.A. and his laboratory were supported by a Human Frontier Science Program Long-Term Fellowship (LT000461/2015-L), a Swiss National Science Foundation Ambizione Grant (PZ00P3 185743) and the Fondation Pierre Mercier pour la science. R.B.'s laboratory was supported by the University of Lausanne, the Swiss National Science Foundation (310030B-185377) and ERC Consolidator (615094) and Advanced (833548) Grants.

Author Contributions

S.T., T.O.A. and R.B. conceived the project. All authors contributed to experimental design, analysis and interpretation of results. Specific experimental contributions were as follows: S.T. performed all calcium imaging, photoactivation, tethered fly behavioural experiments and cloning of the *VT033006-LexA* construct. T.O.A. performed molecular biology experiments, generated transgenic lines, performed histology, Or85b QTL analysis, cell number quantifications and electrophysiology. G.S. performed PN electrophysiology, dye-filling and anatomical analysis, with guidance from J.M.J. L.A. performed molecular biology experiments, histology and quantifications of post-synaptic puncta. S.D.S. performed the wind tunnel behavioural experiments, with guidance from F.v.B. J.R.A. performed the Ir75b QTL analysis and contributed to the Or85b QTL analysis. L.L.P.-G. performed the Ir75b QTL analysis. D.L.S. contributed to the QTL analyses and generated the *UAS-CsChrimson* construct. S.C. contributed to the Ir75b QTL analysis. R.A.O. performed histology in the *D. melanogaster* subgroup. C.F.R.W. generated the parent *SPARC2-TNT* construct. S.T., T.O.A. and R.B. wrote the paper with input from all other authors. All authors approved the final version of the manuscript.

Competing interests

The authors declare no competing interests.

Methods

Data reporting

Preliminary experiments were used to assess variance and determine adequate sample sizes in advance of acquisition of the reported data. For electrophysiological recordings, data were collected from multiple flies on several days in randomised order. Within datasets, the same odour dilutions were used for acquisition of the data. The experimenter was blinded to the genotype for quantification of OSN numbers, and SPARC2-CsChrimson and SPARC2-TNT tethered fly assays, but not for other behavioural or physiological experiments.

Drosophila strains

Drosophila stocks were maintained on standard wheat flour/yeast/fruit juice medium or, for those used in PN electrophysiology experiments, semi-defined culture medium[63] under a 12 h light:12 h dark cycle at 25°C. For all *D. sechellia* strains, a few g of Formula 4-24® Instant *Drosophila* Medium, Blue (Carolina Biological Supply Company) soaked in noni juice (Raab Vitalfood or Tahiti Trader) were added on top of the standard food. Wild-type, mutant and transgenic *Drosophila* lines used in this study are listed in **Extended Data Table 2.**

To generate *lozenge* (*lz*) *trans*-heterozygous *D. simulans/D. sechellia* hybrid flies, we group-aged 25-35 virgin males of *D. simulans* (*Dsim03 Or85b*^{GFP} or *Dsim03 lz*^{RFP}*;Or85b*^{GFP}) for 6-7 days before combining them with 20-30 virgin females of *D. sechellia* (*Dsec07 lz*^{RFP}*;Or85b*^{GFP} or *Dsec07 Or85b*^{GFP}). We lowered the fly food cap to restrict space and force interactions between the animals (which otherwise had a very low tendency to mate). Tubes were maintained at 22°C with strong light exposure and flipped every 3-4 days into a new tube. Progeny were collected and phenotyped 7-10 days post-eclosion.

Constructs for CRISPR/Cas9-mediated genome engineering and transgenesis

D. simulans Or85b: for expression of a single sgRNA targeting the *D. simulans Or85b* locus, an oligonucleotide pair (**Extended Data Table 3**) was annealed and cloned into *BbsI*-digested *pCFD3-dU6-3gRNA* (Addgene #49410) as described[64]. To generate a donor vector for homologous recombination, homology arms (1-1.6 kb) were amplified from *D. simulans* (*Drosophila* Species Stock Center [DSSC] 14021-0251.195) genomic DNA and inserted into *pHD-Stinger-attP*[23] via restriction cloning. Both constructs were co-injected with a source of Cas9 (as described below) into *D. simulans* DSSC 14021-0251.003 and DSSC 14021-0251.004.

D. simulans and *D. sechellia lz*: to express multiple sgRNAs targeting the *lz* loci from the same vector backbone, oligonucleotide pairs (**Extended Data Table 4**) were used for PCR and inserted into *pCFD5* (Addgene #73914) via Gibson Assembly, as described[65]. To generate donor vector for homologous recombination, homology arms (1-1.6 kb) were amplified from *D. sechellia* (DSSC 14021-0248.07) or *D. simulans* (DSSC 14021-0251.195) genomic DNA and inserted into *pHD-DsRed-attP*[66] via Gibson Assembly. Species-specific constructs were co-injected with a source of Cas9 (as described below) into *D. simulans* DSSC 14021-0251.004 or *D. sechellia nos-Cas9*[23].

D. sechellia UAS-SPARC2-D-CsChrimson: we digested a *SPARC2-backbone* vector (Addgene #133562) with *SalI* and inserted a *CsChrimson-Venus* cassette after PCR amplification from *pBac(UAS-ChR2 CsChrimson,3xP3::dsRed)* via Gibson Assembly. The resulting *SPARC2-D-CsChrimson* cassette was amplified via PCR and inserted via restriction cloning into *pHD-3xP3-DsRed DattP-D. sechellia attP40* (this targeting vector for homologous recombination at the *D. sechellia attP40* equivalent site will be described in more detail elsewhere).

D. sechellia UAS-SPARC2-D-TNT-HA-GeCO: we first generated a *pHD-3xP3-DsRed_DattP-UAS-TNT-GeCO* vector by amplifying a *TNT-GeCO* cassette from *pHD-37.1_AttP5_LexAop_90_10_TNT-HA_p2A_jRGeCO1a* together with a *UAS* cassette and insertion into *pHD-3xP3-DsRed DattP* via Gibson Assembly. Subsequently, we transferred the *UAS-TNT-HA-GeCO* cassette into *pHD-3xP3-DsRed DattP-D. sechellia attP40* before assembling *pHD-3xP3-DsRed DattP-D. sechellia attP40 SPARC2-D-TNT-HA-GeCO* via Gibson Assembly (the GeCO calcium indicator was not used in the current study). Both *SPARC-D* transgenic lines in *D. sechellia* were generated via CRISPR/Cas9-mediated homologous recombination at the *attP40*-equivalent site in *D. sechellia*. To test the functionality of the *UAS-TNT-HA-GeCO* cassette, we also generated *UAS-TNT-HA-GeCO* transgenic lines via homologous recombination at the *attP40* locus in *D. melanogaster* and *D. sechellia*. However, in both species successful transformants did not survive pupariation, which was potentially due to low-level, Gal4-independent expression of the TNT effector.

D. melanogaster VT033006-LexA: to generate a *VT033006-LexA* construct, *pLexA-SV40-attB* was digested with *NotI*. A *VT033006* enhancer fragment was PCR-amplified from *pVT033006-Gal4-attB*[39]. The insert and the linearised vector were joined by Gibson assembly. The vector was integrated into *D. melanogaster attP2* by BestGene Inc.

D. sechellia VT033006-Gal4, *VT033008-Gal4* and *VM5d-Gal4*: constructs carrying the *D. melanogaster* enhancer sequences[39] were integrated into *Dsec-white* (attP landing site on the X chromosome[23]) or *Dsec-attP40* (see next section). The *Dsec-nSyb-ΦC31* line was generated by integration of *nSyb-ΦC31* (Addgene #133868) into *Dsec-attP26* (see next section).

D. sechellia UAS-myrGFP: pUAS-myrGFP, QUAS-mtdTomato(3xHA)[67] was integrated into *Dsec-attP40*. *D. sechellia UAS-Dα7:*GFP: flies were generated by P-element-mediated transgenesis of *p(UAS-Dα7:GFP)*[43] into *D. sechellia* DSSC 14021-0248.30 by WellGenetics.

D. sechellia pBac(UAS-CsChrimson-Venus): we first amplified a *UAS-CsChrimson-Venus* cassette from *pUAS-ChR2 CsChrimson*[68] and a *pBac* backbone[69] and combined both via Gibson assembly resulting in *pBac(UAS-CsChrimson-Venus)*. Subsequently, we digested *pBac(UAS-CsChrimson-Venus)* with *AscI*, amplified a *3xP3-DsRed* cassette (derived from gene synthesis, Genetivision) via PCR and combined both via Gibson Assembly resulting in *pBac(UAS-CsChrimson-Venus,3xP3-DsRed)*. Primer sequences for intermediate cloning steps are listed in **Extended Data Table 3**. PiggyBac-mediated transgenesis of *pBac(UAS-CsChrimson-Venus,3xP3-DsRed)* into *D. sechellia* DSSC 14021-0248.07 was performed in-house (see below) and the insertion site mapped to the third chromosome using TagMap[70]. Beyond its use for optogenetic experiments, we took advantage of the visible 3xP3-DsRed marker to use the same line for introgression mapping (**Extended Data Figure 2c,d**).

All plasmids were verified via Sanger sequencing before injection. Full details and oligonucleotide sequences are available from the corresponding authors upon request.

Drosophila transgenesis

Except for specific constructs described above, mutagenesis/transgenesis of *D. sechellia*, *D. simulans* and *D. melanogaster* was performed in-house following standard protocols[23] *.* For *piggyBac* and P-element transgenesis, we co-injected a *piggyBac* or *P-element* vector (300 ng μl^{-1}) and *piggyBac*[71] or *P-element* helper plasmid[72] (300 ng μl^{-1}). For CRISPR/Cas9-mediated homologous recombination, we injected a mix of an sgRNA-encoding construct (150 ng μl^{-1}) and donor vector (500 ng μl^{-1}) into *D. sechellia nos-Cas9*[23] or co-injected with *pHsp70-Cas9* (400 ng μl^{-1}) (Addgene #45945*;* for *D. simulans* transgenesis)[73]. Site-directed integration into *attP* sites was achieved by co-injection of an *attB*-containing vector (400 ng μl^{-1}) and *pBS130* (encoding *Φ*C31 integrase under control of a heat shock promoter (Addgene #26290)[74]). The *Dsec-attP26* site (on chromosome 4) was generated via *piggyBac*-mediated random integration and *Dsec-attP40* via CRISPR-mediated homologous recombination and both will be described in more detail elsewhere. All concentrations are given as final values in the injection mix.

Histology

Fluorescent RNA *in situ* hybridisation (using digoxigenin- or fluorescein-labelled RNA probes) and immunofluorescence on whole-mount antennae were performed

essentially as described[75,76]. Probes were generated using *D. sechellia* genomic DNA (*Or47a*, *Or88a*) and primers listed in **Extended Data Table 3**. Other published probes were either targeting *D. sechellia* (*Or42b*, *Or22a*, *Or85b*, *Or13a*, *Or98a*, *Or35a*[23]), *D. simulans* (*Or67a*[77]) or *D. melanogaster* transcripts (*Or56a*, *Or59b, Or9a*, *Or69aA*[78]; *Or19a*[19]; *Or83c*, *Or67d*[28]); all probes were used at a concentration of 1:50. Immunofluorescence on adult brains – with the exception of the visualisation of dye-filled PN (described below) – was performed as described[79].

The following antibodies were used: guinea pig α-Ir75b 1:500 (RRID:AB_2631093[22]), mouse monoclonal antibody nc82 1:10 (Developmental Studies Hybridoma Bank), rabbit α-GFP 1:500 (Invitrogen), and rat α-HA 1:500 (Roche). Alexa488-, Cy3- and Cy5-conjugated goat α-guinea pig, goat α-mouse, goat α-rabbit and goat α-rat IgG secondary antibodies (Molecular Probes; Jackson Immunoresearch) were used at 1:500.

Image acquisition and processing

Except for dye-filled PN imaging and analysis (described below), confocal images of antennae and brains were acquired on an inverted confocal microscope (Zeiss LSM 710) with an oil immersion 40× objective (Plan Neofluar 40× Oil immersion DIC objective; 1.3 NA). For quantification of synapse numbers, images were taken using a 63× objective (Plan-Apochromat 63× Oil immersion DIC M27; 1.4 NA) with a zoom of 3×, centring the image on the glomerulus of interest. Images were processed in Fiji[80]. *D. sechellia* brains were imaged and registered to a *D. sechellia* reference brain[23] using the Fiji CMTK plugin (https://github.com/jefferis/fiji-cmtk-gui).

Cell number quantification: the number of OSNs expressing a specific *Or* was quantified using Imaris (Bitplane) or the Fiji Cell Counter tool. For GFP-expressing Or85b OSNs for the QTL analysis, we imaged GFP and, in the 568 nm channel, cuticular autofluorescence. After subtraction of the cuticular fluorescence signal from the GFP signal using the Subtraction tool in Fiji, we quantified the number of GFP-positive nuclei using the Surface Detection tool in Imaris. For Ir75b neurons, we found that α-Ir75b immunofluorescence resulted in labelled cells having a range of intensities. To ensure that the cell quantifications were reproducible, counting was performed manually by three experimenters. Images resulting in disagreements were re-checked and either resolved or removed from the analyses.

Glomerular and synapse quantification: glomerular volumes were calculated following segmentation with the Segmentation Editor plugin of Fiji using the 3D Manager plugin. The number of post-synaptic sites per glomerulus was quantified in Imaris as described[38], setting punctum size to 0.45 μm^3 for all images.

Quantitative trait locus mapping

Or85b phenotyping: flies expressing nuclear-localised GFP in Or85b neurons were placed individually into 96-well plates whose bottom was replaced by a metal mesh. Antennae were removed via shock-freezing in liquid nitrogen and collected in 4% paraformaldehyde-3% Triton-PBS as described[75]. After 3 h of fixation, antennae were washed twice in 3% Triton-PBS and twice in 0.1% Triton-PBS and mounted in Vectashield (Vectorlabs) on 30-well PTFE printed slides (Electron Microscopy Sciences) before imaging on a Zeiss LSM710 confocal microscope. The fly bodies were transferred (by inversion) into separate 96-well plates and frozen at -20°C.

Genomic DNA of individual flies was extracted using the ZR-96 Quick-gDNA MiniPrep kit (Zymo Research).

Ir75b phenotyping: flies were processed as described above. For antennae, after washing in 0.1% Triton-PBS, Ir75b immunofluorescence was performed. Antennae were mounted in Vectashield (Vectorlabs) on 30-well PTFE printed slides (Electron Microscopy Sciences) before imaging on a Zeiss LSM710 confocal microscope.

Sequencing and genotyping: genomic DNA of individual flies was tagmented with in-house produced Tn5 as described[81]. In brief, Tn5 was charged with adaptors and mixed at a concentration of 5 ng μl^{-1} with 1 μl of genomic DNA. After tagmentation, Tn5 was de-activated by addition of 0.2% sodium dodecyl-sulphate and sample specific sequencing adaptors were added by PCR amplification. The resulting PCR amplicons were cleaned-up with AMPure XP bead-based reagents (Beckman Coulter Life Science), DNA concentration and fragment distribution quantified on a fragment analyser (Agilent) and single-end sequenced on an Illumina HiSeq sequencer.

Data analysis: to align sequencing reads, the parental genomes dsim r2.02 and dsec r1.3 were used as reference. Introgressed genomic regions were inferred using MSG software (http://www.github.com/JaneliaSciComp/msg). Output of MSG was thinned using the "pull_thin" utility (http://www.github.com/dstern/pull_thin) and read into R (v4.4.1) using the "read_cross_msg" utility (http://www.github.com/dstern/read_cross_msg). QTL mapping was carried out with the qtl package (v1.5) using the Haley-Knott method and significance was determined using 1000 permutation tests (n.perm = 1000). For the Or85b mapping experiment, tests for interactions between the QTL on chromosomes 3 and X were performed using the "fitqtl" function.

Two-photon calcium imaging

Animal preparation: flies of the appropriate genotype (described in the respective figure legends) were collected (females and males co-housed) and reared in standard culture medium (see above, with an addition of blue food with noni juice for *D. sechellia*). Female flies aged 5-8 days after eclosion were used for the experiments.

Sample preparation: flies were anaesthetised by placing them into an empty vial that was cooled on ice for no longer than ~10 min. Further steps were performed under a dissection microscope, adapting a previous protocol[82]. A small drop of blue light-curing glue (595987WW, Ivoclar Vivadent) was placed on top of the copper grid (G220-5, Agar Scientific). Single flies were introduced into the mounting block fixing the back of the fly head to the copper grid with the curing glue. The fly head was slightly bowed down with forceps (to achieve antennal lobe imaging from the dorsal side) while the blue curing light (bluephase C8, Ivovlar Vivadent; placed at least 1 cm from the fly to avoid tissue damage) was focused. We avoided using the wire that was previously used to pull down the antennal plate[23,82], as we found that it very frequently damaged the antennal nerves and therefore disrupted central olfactory responses, particularly in *D. sechellia*; the cactus spine and screw previously used to immobilise the fly head were also no longer necessary. An antennal shield[82] was placed over the top of the fly head with the hole positioned centrally, fixed with beeswax to the top of the mounting block. Two-component silicon (Kwik-Sil, World Precision Instruments) was mixed with a toothpick and poured into the hole of the antennal shield to seal the gap between

the plate and the fly head, avoiding any leakage onto the antennae. As the silicon was left to harden (during 10-15 min), we used blunt forceps to gently remove silicone on the cuticle on top of the head capsule. A drop of adult haemolymph (AHL) saline (108 mM NaCl, 5 mM KCl, 2 mM $CaCl_2$, 8.2 mM $MgCl_2$, 4 mM $NaHCO_3$, 1 mM NaH_2PO_4, 5 mM trehalose, 10 mM sucrose, 5 mM HEPES, pH 7.5) was added into the hole of the antennal shield. Using a blade-splitter, a small rectangular hole was cut in the head cuticle between the eyes and above the antennal plate. Tracheae and glands above the brain were removed with fine forceps. Finally, the brain was rinsed with AHL saline at least 3 times until the antennal lobe appeared clear under the dissection microscope.

Odorant preparation: serial dilutions of odours were prepared in a fume hood. The solvents used for odour dilutions were different between glomeruli, as some glomeruli were extremely responsive to particular solvents: Or85b/VM5d (*2*-heptanone (CAS 110-43-0) in dichloromethane (DCM)), Or22a/DM2 (methyl hexanoate (CAS 106-70-7) in paraffin oil), Or59b/DM4 (methyl butyrate (CAS 623-42-7) in DMSO (for dose-responses) or paraffin oil (for pulsed stimuli)), Or92a/VA2 (*2*,*3*-butanedione (CAS 431-03-8) in paraffin oil). Or85b/VM5d neurons were especially sensitive to odorant contamination, so we prepared a new set of *2*-heptanone dilutions when solvent responses started to become evident (approximately every two weeks). Furthermore, before preparing *2*-heptanone and methyl butyrate, we washed the odour-containing vial, lid and pipetting tips with DCM and DMSO, respectively. As DCM is highly volatile at room temperature, *2*-heptanone/DCM odour dilutions were stored at 4°C.

Image acquisition: images were acquired using a commercial upright two-photon microscope (Zeiss LSM 710 NLO). An upright Zeiss AxioExaminer Z1 was fitted with a Ti:Sapphire Chameleon Ultra II infrared laser (Coherent) as excitation source. Images were acquired with a 20× water dipping objective (Plan-Apochromat 20× W; NA 1.0), with a resolution of 128×128 pixels (0.8926 pixels μm^{-1}) and a scan speed of 6.30 µs $pixel^{-2}$ (for one-time odour stimulation) or 3.15 s $pixel^{-2}$ (for pulse train odour stimulation). The excitation wavelength was set to 930 nm. The output power was modified according to the baseline fluorescence of GCaMP6f, which varied substantially between animals (except for pharmacology experiments, where laser output was consistent to enable comparison of raw fluorescence across animals). The power was set such that the baseline fluorescence was above the detection limit, and that the maximum fluorescence was below saturation, and thereafter unchanged for a given animal. Emitted light was filtered with a 500-550 nm band-pass filter, and photons were collected by an internal detector. Each measurement consisted of 50 images acquired at 4.17 Hz (for one-time odour stimulation) or 8.34 Hz (for pulse train odour stimulation), with stimulation starting ~5 s after the beginning of the acquisition and lasting for 1 s (for one-time odour stimulation) or 200 ms followed by a 200 ms interval repeated ten times (for pulse train odour stimulation).

Olfactory stimulation: antennae were stimulated using a custom-made olfactometer[23,82]. In brief, antennae were permanently exposed to air flowing at a rate of 1.5 l min^{-1} by combining a main airstream of humidified room air (0.5 l min^{-1}) and a secondary stream (1 l min^{-1}) of normal room air. Both air streams were generated by vacuum pumps (KNF Neuberger AG) and the flow rate was controlled by two independent rotameters (Analyt). The secondary airstream was guided either through an empty 2 ml syringe or through a 2 ml syringe containing 20 µl of odour or solvent on a small cellulose pad (Kettenbach GmbH) to generate odour

pulses. To switch between control air and odour stimulus application, a three-way magnetic valve (The Lee Company, Westbrook, CT) was controlled using MATLAB via a VC6 valve controller unit (Harvard Apparatus). The order of the odour stimuli was always from lower to higher concentrations, preceded by the solvent control. Successive odour stimulations were separated by 1 min intervals.

Pharmacology: for pharmacological experiments, drugs were diluted in AHL saline to the following final concentrations: 100 µM Picrotoxin (P1675-1G, Sigma-Aldrich, CAS 124-87-8), 50 µM CGP54626 hydrochloride (1088/10, TOCRIS, CAS 149184-21-4), 200 µM (low dose) or 2 mM (high dose), mecamylamine hydrochloride (M9020-5MG, Sigma-Aldrich, CAS 826-39-1). Drugs were applied to the fly after normal recording ("saline / naïve") by exchanging the AHL saline with drug-diluted saline five times and incubating the preparation for a further 15-40 min before performing further recordings. For mecamylamine application experiments, samples were subsequently washed with AHL saline five times and incubated for 15-40 min, followed by another recording session ("Washed-out"). The lens was meticulously washed with ultrapure water between each session.

Data analyses: data were processed using Fiji and custom written scripts in R. First, the image stacks were passed through the StackReg plugin[83] (transformation: Rigid Body) to correct for movement artefacts. Using Fiji, a circular region of interest (ROI) was set within the glomerulus of interest on the left half of the brain image (except when the signal was weak, in which case the right half of the image was used). The signal intensity averaged across the ROI for each timeframe (hereafter F) was used to calculate the normalised signal $\Delta F/F_0 = \frac{F-F_0}{F_0}$. Here, F_0 (baseline fluorescence) was calculated as the average F during frames 16-19 (1 s before olfactory stimulus onset). The peak $\Delta F/F_0$ value (which represents the odour response intensity) was calculated as the maximum $\Delta F/F_0$ value during frames 20-23 (1 s during olfactory stimulation). We noticed that the maximum $\Delta F/F_0$ value itself was often very different between species/genotypes, presumably due to different expression levels of GCaMP6f. This should, in theory, not affect the normalised $\Delta F/F_0$ value, but we did observe a saturation of neuronal responses above a certain odour concentration, even if the peak $\Delta F/F_0$ value was lower than in other species/genotypes. To compare the dose-response effect between species and genotypes, we further introduced a normalisation step. Normalised peak response for each odour dilution ($\tilde{p}$) was calculated as follows: $\tilde{p} = \frac{p-p_0}{p_{max}-p_0}$. Here, p denotes peak $\Delta F/F_0$ value of a given dilution (median value across animals), p_{max} denotes maximum p among all the dilutions, and p_0 denotes p from the minimum response. Thus, the normalised peak response $\tilde{p}$ takes a value between 0 and 1, where 0 means absence of odour responses and 1 means saturation. This step allowed us to compare the dose-response curve based on the relative response within species and genotypes, regardless of the absolute $\Delta F/F_0$ value. Dynamic ranges were quantified as $p_{max} - p_0$ in each animal rather than taking the median values across animals.

Photoactivation

Animal preparation: flies of the appropriate genotype (see figure legends) were collected, reared and prepared in the same way as for the two-photon calcium imaging. Female flies aged 6-9 days after eclosion were used for the experiments.

Photoconversion and image acquisition: the hardware setup was the same as in two-photon calcium imaging. Glomerular location was identified by a brief 930

nm scan of the entire antennal lobe. An oval ROI was placed inside the glomerulus of interest, where the ROI was made small enough so that the movement during photoconversion did not result in non-specific labelling. Where non-specific labelling was observed after imaging, data were excluded from further analyses. During photoconversion, the resolution was set to 512×512 pixels (3.5704 pixels μm^{-1}) and the scan speed to 0.79 µs $pixel^{-2}$. Excitation wavelength was shifted to 760-780 nm with a power output of 5-15%. Photoconversion was performed by scanning inside the ROI repeatedly (in a single z-plane) for ~15 min. Around 5 min after the beginning of the session, a brief 930 nm scan was performed to check the conversion efficacy and specificity. If photoconversion was weak at this point, we increased the power output. The sample was then placed in a humidified chamber for 30-60 min to allow the diffusion of photoconverted C3PA-GFP. Finally, the fly's body was removed to reduce motion artefacts and the sample placed again under the two-photon microscope. For imaging, the resolution was set to 1024×1024 pixels (2.3803 pixels μm^{-1}) and the scan speed to 1.58-3.15 µs $pixel^{-2}$. The excitation wavelength was shifted back to 930 nm with the power output adjusted to enable visualisation of neurite processes. Z-stack images were obtained with a spacing of 1 µm.

Electrophysiology

Single sensillum recordings: single sensillum electrophysiological recordings were performed essentially as previously described[23], using 5-7 day-old female flies, which were grown on standard medium mixed with 0.2 mM all-*trans* retinal[68], and, for *D. sechellia*, addition of 10% noni juice. Optogenetic stimulation was performed by exposing one antenna with increasing light intensities via an optic fibre as described in the **Tethered fly assay** section (see below). In SPARC2 experiments, ab3 sensilla were identified by location and the use of diagnostic odours. For the data shown in **Fig. 3c**, light-sensitive (experimental group) and non-responding neurons (control) were analysed. Corrected responses were calculated as the number of spikes in a 0.5 s window from the beginning of illumination, subtracting the number of spontaneous spikes in a 0.5 s window 2 s prior to illumination, and multiplying by 2 to obtain spikes s^{-1}. Recordings were performed on a maximum of three sensilla per fly. Exact *n* values and mean spike counts for all experiments are provided in **Extended Data Table 1**.

Whole-cell patch clamp recordings: for *in vivo* VM5d PN recordings, flies were prepared and dissected as previously described[47]. Female flies aged 1-2 days post-eclosion were used for the experiments; one neuron was recorded per brain. The internal patch pipette solution contained 140 mM potassium aspartate, 10 mM *4*-(*2*-hydroxyethyl)-*1*-piperazineethanesulfonic acid, 4 mM MgATP, 0.5 mM Na_3GTP, 1 mM ethylene glycol tetraacetic acid, 1 mM KCl and, for cell labelling described below, 13 mM biocytin hydrazide. The pH was adjusted to 7.3, and the osmolarity was adjusted to ~265 mOsm. The external saline contained 103 mM NaCl, 3 mM KCl, 5 mM *N*-tris(hydroxymethyl) methyl-*2*-aminoethane-sulfonic acid, 8 mM trehalose, 10 mM glucose, 26 mM $NaHCO_3$, 1 mM NaH_2PO_4, 1.5 mM $CaCl_2$, and 4 mM $MgCl_2$. The osmolarity was adjusted to 270-273 mOsm, and the saline was bubbled with 95% O_2 and 5% CO_2 and reached an equilibrium pH of 7.3. Saline was continuously superfused over the fly during recording. Recordings were acquired with an Axopatch 700B or 200B model amplifier, low-pass filtered at 4 or 5 kHz, and digitized at 10 kHz. Patch pipettes, made from borosilicate glass, were

pressure-polished. The estimated final pipette tip opening was less than 1 μm in diameter, and the pipette resistance was 15-45 MΩ.

Olfactory stimulation: serial dilutions of *2*-heptanone (in mineral oil) were freshly prepared before each experiment. A custom-made olfactometer was used to deliver odour to flies. Antennae were consistently exposed to a stream of air at 363 ml min^{-1}. Another stream of air (5.3 ml min^{-1}) was directed through a solenoid valve into a 2 ml vial (Thermo Scientific, National C4011-5W) containing either mineral oil alone or an odour solution in mineral oil. Odour delivery, controlled by a custom MATLAB script and a three-way solenoid valve (The Lee Company, Westbrook, CT), lasted 2 s. The series of stimuli always started with the solvent control followed by increasing odour concentrations. Custom-written MATLAB scripts were used to detect spikes based on the first derivative of the voltage trace. A threshold was set for each recording and all spikes were visually inspected to eliminate both false positive and false negative detections. The spike time was defined as the time of the peak of the first derivative of the voltage waveform. An average of three trials was taken for each concentration for each cell. Corrected responses were calculated as the spike rate in a 50 ms (**Fig. 5e and Extended Data Fig. 7b**) or 500 ms (**Extended Data Fig. 7b**) window and subtracting the spontaneous spike rate (computed in a 500 ms window 2 s prior to stimulation). Exact *n* values and mean spike counts for all experiments are provided in **Extended Data Table 1**.

Projection neuron backfilling and reconstruction: each brain was dissected out of the head capsule after the recording and fixed with 4% PFA (w/v) in PBS for 20 minutes at room temperature. After washing with PBS-T [PBS with 0.2% (v/v) Triton X-100 (Sigma Aldrich, #X100)], brains were incubated with streptavidin Alexa Fluor 568 (1:1000) (Invitrogen S11226) and nc82 (1:50) and 10% Normal Goat Serum in 0.2% PBS-T overnight at RT. The brains were washed and incubated with streptavidin Alexa Fluor 568 (1:1000) and anti-mouse Alexa Fluor 633 (1:500) and 10% Normal Goat Serum in 0.2% PBS-T overnight. After the final wash with PBS, brains were mounted in Vectashield H-1000 (Vector Laboratory, Burlingame, CA) anti-fade mounting medium for confocal microscopy. Brains were imaged with a Zeiss LSM880 confocal microscope. Confocal images displayed Biocytin fills in all recordings, and dendritic surface area was measured using IMARIS 10.0.0 (Bitplane) through a semi-automated generation of surfaces for each dendritic arbour.

For one *D. melanogaster* recording, the biocytin fill revealed two coupled cells: one innervating the VM5d glomerulus and the other innervating a different glomerulus. Correspondingly, two distinct spike waveforms were clearly discernible in the voltage trace. We excluded this recording from membrane voltage and input resistance analyses but included it in spike rate analysis because the VM5d PN spikes could be identified by their clear responses to *2*-heptanone. The VM5d arbour in this fill was included in the dendritic morphology analysis.

Tethered fly assay

Assay: the assay was built on a solid breadboard (Thorlabs). The fly tether was made by inserting and gluing an insect pin (Austerlitz, φ = 0.20 mm) to a 200 μl pipette tip, which was mounted on a magnetic articulated stand (NOGA). Two microphones (lavalier microphone, RODE) were placed ~1 mm from the tip of the wings of the fly, connected to a USB audio interface (Rubix 22, Roland) via TRS-XLR adaptors (VXLR, RODE). The audio interface was connected to Raspberry Pi

computer (Raspberry Pi 4 1.5 GHz Quad-Core, 8GB RAM), which ran the real-time feedback programme (described below) based on the acoustic inputs. The output of the feedback system was SPI-connected to a DotStar LED strip (1528-2488-ND, Adafruit; cut to 30 LEDs), which was bent to make a U-shape that covers >180° of the fly's horizontal view. The spatial frequency of the visual guide was set to ~0.036 mm^{-1} (one illumination in every 4 LEDs). The PTFE odour port was placed at ~30° from the right side, facing the fly ~1 cm apart to provide unilateral olfactory stimulation. The suction port was placed at the opposite end of the odour port, ~2 cm from the fly, to stabilise the odour plume. For optogenetic experiments, single antennae were illuminated using a custom-made optic fibre (G050UGA, Tubing: FT030, End 1: SMA, End 2: Flat Cleave, Thorlabs), of which the cleaved end was placed ~0.1 mm from one antenna. The position of the optic fibre was adjusted using a 3D microcontroller (UM-3C, Narishige), and was monitored by a Pi NoIR camera prior to each session. The fibre was connected to 660 nm fibre-coupled LED (M660FP1, Thorlabs) via a compact LED driver (LEDD1B, Thorlabs).

Real-time feedback system: the feedback system was run by a custom Python script. The recording was performed binocularly from each wing at the rate of 44,100 Hz. Each session (20 s) was divided into 0.1 s intervals. The raw wing beat amplitude ($r_{[L]}$, $r_{[R]}$) was defined by the difference between the maximum and minimum sound amplitude within each interval. The raw wing beat was filtered by calculating the median across the three most recent intervals ($r_{f[L]}$, $r_{f[R]}$). Prior to the experimental session, each fly was calibrated by a "mock" session, where the visual guide was fixed and the flies beat their wings to obtain the mean ($\mu_{mock[L]}$, $\mu_{mock[R]}$) and SD ($\sigma_{mock[L]}$, $\sigma_{mock[R]}$) of the filtered wing beat amplitude as well as the SD of the difference between the left and right wing beat amplitudes ($\sigma_{mock[L-R]}$). In the experimental sessions, the filtered raw wing beat amplitudes were standardized using the mean and SD obtained in the mock session ($z_{[L]}=\frac{r_{f[L]}-\mu_{mock[L]}}{\sigma_{mock[L]}}$, $z_{[R]}=\frac{r_{f[R]}-\mu_{mock[R]}}{\sigma_{mock[R]}}$). The ΔWBA was defined by $z_{[L]}$-$z_{[R]}$ as a readout of turning behaviour. In each interval, the visual guide was rotated counter-clockwise (shifting by one adjacent LED) if $\Delta WBA > 3\sigma_{mock[L-R]}$ and clockwise if clockwise if $\Delta WBA < 3\sigma_{mock[L-R]}$. The $z_{[L]}$, $z_{[R]}$ values were saved after each session for downstream analyses.

Animal preparation: flies of the appropriate genotype were collected (females and males co-housed). For odour response experiments, females 5-9 days after eclosion were used (except for SPARC2-D-TNT experiments, where flies were 0-1 day old since the experimental group did not survive for long). For experiments with apple cider vinegar (Migros, M-Classic), flies were starved for 5-7 h. Fly rearing for optogenetic experiments is as described in **Electrophysiology** section. Flies were reared in retinal-containing food for 6-7 days, and females 6-8 days after eclosion were used.

Sample preparation: flies were anaesthetised on ice and attached to the fly tether using blue-curing glue. For optogenetic experiments, fly forelegs were cut to prevent the flies from perturbing the optic fibre. The fly tether was mounted on a magnetic stand, and the fly positioned centrally and equidistantly between the microphones. For optogenetic experiments, videos were taken during positioning of optic fibres to confirm that the illumination (at intensity 3, as described below) was confined to one antenna. For SPARC2-D-TNT-HA experiments, as transgene

expression was not detected in a fraction of flies (for unknown reasons), post-hoc HA immunofluorescence was performed in individual antennae and/or brains and the behavioural data for animals with positive labelling in OSN cell bodies and/or axon termini were retained in the downstream analyses.

Olfactory stimulation: odorants (5 ml) were contained in 15 ml Falcon tubes with two syringe needles pierced at the lid. Tubes were connected to the syringe needle outlets to provide odour stimulation from the headspace. The flies were permanently exposed to water vapour at a rate of 0.5 l min^{-1}. A three-way magnetic valve (The Lee Company, Westbrook, CT) was controlled using MATLAB via a VC6 valve controller unit (Harvard Apparatus) to switch the airflow from water to odorants. Either 10 consecutive pulses of 500 ms with 500 ms intervals or a single 10 s pulse were used as olfactory stimuli. Noni juice was diluted in water while benzaldehyde was diluted in paraffin oil.

Optogenetic stimulation: LED illumination was controlled by sending TTL signals to the LED driver. 10 consecutive pulses of 500 ms with 500 ms intervals were used. The intensity of the illumination was modified by the dial on the LED driver, which could be modulated from intensity 0 (mock-stimulation) to 6 (maximum). Intensity 4 was used for stimulation in most experiments, except for low-intensity stimulation (intensity 3) to match the OSN spike rate with SPARC2-D-CsChrimson experiments. For SPARC2-D-CsChrimson experiments, we noticed that the animals either displayed expression of CsChrimson (as detectable by the Venus tag) in about half of the Or22a OSN population or had no expression at all. The reason for this heterogeneity is unknown but we performed post-hoc imaging of Venus fluorescence in individual antennae of all animals to analyse data from only those that expressed the transgene.

Data analyses: data were analysed with custom programmes in R. The quantification was performed in 1 s time windows corresponding to pre-stimulus baseline (4-5 s) and individual odour-pulse responses (1st peak: 5-6 s, 2nd peak: 6-7 s, …, 10th peak: 14-15 s). For quantification of *ΔWBA* in each time window, the *ΔWBA* values above the 50% quantile were used, to avoid picking outliers and non-attractive epochs.

Wind tunnel assay

Free flight tracking was performed in a 1 m × 0.5 m × 0.5 m wind tunnel housed in a temperature- and humidity-controlled room (22°C, 60% RH). The wind tunnel floor was illuminated by blue LEDs underneath a light-diffusive film that lined the tunnel floor, overlaid with a grid of infrared transmissible film; this grid formed a checkerboard-like lattice on the floor to provide flies with ventral optic flow information. The walls of the wind tunnel tapered from blue on the floor to black along the ceiling. Along the top of the wind tunnel were two white LED strips, to provide sufficient orange light for *Drosophila* photoreceptor re-isomerisation[84]. Total illumination in the wind tunnel was 452 Lux as measured from the wind tunnel centre (LX1330B light sensor, Dr. Meter).

Fly tracking was performed with 12 synchronised Basler acA720 cameras (Basler AG, Ahrensburg) recording at 100 Hz (**Extended Data Fig. 4a**). The walls and floor of the wind tunnel were homogenously illuminated with arrays of infrared LEDs, and cameras were outfitted with IR pass filters to track flies using only infrared wavelengths. Tracking was performed using Braid software[32]. Odour plumes were introduced in the wind tunnel through an odour port constructed from a 20 cm tall rigid acrylic tube that had a 90° bend towards the top so that its outward

facing opening was parallel to the wind (**Extended Data Fig. 4b**). The odour port was installed on the far upwind end of the tunnel and its open face was covered by an aluminium mesh to prevent flies from entering the odour plumbing. Plumes were generated by fluxing air through a mass flow controller (Alicat Scientific, Tuscon) at 200 cm^3 min^{-1}. The air was then bubbled into 150 ml noni juice at the bottom of a jar and subsequently through tubing leading to the odour port in the wind tunnel.

For wind tunnel experiments we used 3-7 day old female flies. 15 animals were collected in the morning and starved by placing them into a tube containing a moist Kimwipe for 8 h. The flies were placed in the wind tunnel with a 40 cm s^{-1} air flow and tracking initiated. Flies were allowed to fly about the wind tunnel volume for 16-20 h before the recording was terminated the following day.

Data analyses: data were analysed using Python (v3.11). We first filtered out all trajectories from flies that were walking on the tunnel floor or ceiling to focus analyses on flying animals. Our trajectory inclusion criteria were: (i) >500 ms long; (ii) >10 cm in the horizontal plane; (iii) a median position of >5 cm away from any of the tunnel walls; (iv) passed within a 10 cm radius of where the odour plume was aligned in the y-z plane (this excluded flies that simply transited the wind tunnel along the ceiling, far away from the plume).

To analyse the radial distance from the plume, we binned the point cloud generated by all trajectories into 5 cm thick cross-sections, beginning 5 cm downwind of the plume source. We then pared the point cloud further to 10 cm above and below the plume ($0.1<z<0.3$) to isolate trajectory portions that were most likely interacting with the plume (**Extended Data Fig. 4e**), for analyses with or without this restriction. Based on the occupancy maps of trajectories in space from both wild-type *D. sechellia* and *D. melanogaster*, we assumed that the plume sank by 5 cm from the odour nozzle to the end of the wind tunnel and calculated the plume centreline using this mode (for comparisons of straight versus sloped plume models see **Extended Data Fig. 4e-f**). From each of the segmented point clouds we report the mean as the mean of all points, independent of trajectories that contributed to them. Results were robust to whether we instead analysed each trajectory as an independent sample. For course direction distributions, we included only the point cloud within a 3 cm radius of our estimated plume volume, and calculated the kernel densities of the course direction of all points within the estimated plume volume. We further divided the data to the point cloud in the downwind half of the wind tunnel, where trajectories typically began, and the upwind half of the wind tunnel, terminating 5 cm downwind of the plume's origin.

Statistics and reproducibility

Data were analysed and plotted using Excel, R (v3.2.3; R Foundation for Statistical Computing, Vienna, Austria, 2005; R-project-org), MATLAB (2023a), GraphPad Prism (10.1.1) and Python (v3.11).

Data, code and biological material availability

All relevant data supporting the findings of this study are included as source data or available from the corresponding authors upon request. Code used for analyses and all unique biological materials generated in this study are available from the corresponding authors upon request.

Figure Legends

Figure 1: Selective expansion of noni-sensing olfactory sensory neuron populations is a complex developmental trait.

a, *D. sechellia* specialises on noni fruit compared to the generalists *D. simulans* and *D. melanogaster*. Ma, million years ago.

b, Left top, schematic of the drosophilid third antennal segment covered by sensilla of diverse morphological classes and housing the sacculus. Left bottom, antennal basiconic 3 (ab3) sensilla house two neurons expressing the odorant receptor Or22a (and Or22b in *D. melanogaster* and *D. simulans*; this paralog is lost in *D. sechellia*) in the A neuron (hereafter, "Or22a neuron") and Or85c/b in the B neuron (both paralogs are co-expressed; hereafter, "Or85b neuron"). Right, antennal *Or22a/(b)* and *Or85b* expression in *D. sechellia* (*Drosophila* Species Stock Center (DSSC) 14021-0248.07, females) and *D. simulans* (DSSC 14021-0251.004, females). Scale bar, 25 µm. In addition to ab3 sensilla (dashed line), Or85b is expressed in ~10 spatially-segregated OSNs in ab6 sensilla in all three species (**Extended Data Fig. 1b**).

c, Comparison of olfactory sensilla numbers in *D. melanogaster* (*Canton-S*), *D. simulans* (DSSC 14021-0251.004) and *D. sechellia* (DSSC 14021-0248.07) (all females) as assessed by RNA FISH using a diagnostic *Or* probe (grey background) for each sensillum class. Data for Ir-expressing coeloconic sensilla and sacculus chamber 3 (sac3) neurons are from[22]; Ir75d neurons common to ac1, ac2 and ac4 sensilla are not shown. In this and all following panels, box plots show the median and first and third quartiles of the data, overlaid with individual data points. Wilcoxon signed-rank test with comparison to *D. melanogaster*. NS, not significant ($P > 0.05$); *$P < 0.05$; **$P < 0.01$; ***$P < 0.001$.

d, Reciprocal hemizygosity test of the *Or22a/(b)* and *Or85c/b* loci for contributions to species-specific OSN numbers in *D. simulans*/*D. sechellia* hybrids. Using RNA FISH to quantify numbers of *Or22a/(b)* and *Or85b* expressing OSNs in the indicated genotypes ("*Dsec* +" = *D. sechellia.07* wild-type, "*Dsim* +" = *D. simulans.04* wild-type, "*Dsec* -" = *DsecOr22a*^{RFP} or *DsecOr85b*^{GFP}, "*Dsim* -" = *DsimOr22a/b*^{RFP} or *DsimOr85b*^{GFP}), no allele-specific expression differences were observed at either loci. Wilcoxon signed-rank test with comparison to wild-type hybrids. NS, not significant ($P > 0.05$).

e, Quantification of GFP-expressing neurons in antennae of *DsecOr85b*^{GFP}, *DsimOr85b*^{GFP} and F1 hybrid males and females, and in the F2 progeny of the backcrosses of F1 hybrid females to either parental strain. The black line indicates the mean cell number.

f, Logarithm of odds (LOD) score across all four chromosomes for loci impacting Or85b neuron numbers based on the phenotypic data in **e**. Dashed horizontal lines mark $P = 0.05$; non-dashed horizontal lines mark $P = 0.01$.

g, Effect sizes for the significant QTL intervals on chromosome 3 and X in the *D. simulans* backcross. A, *D. simulans* allele; B, *D. sechellia* allele. A candidate gene, *lozenge* – encoding a transcription factor involved in sensilla specification development[85] – that is located directly below the highest score of our trait map on the X chromosome, did not affect OSN numbers (**Extended Data Fig. 2e-i**).

Figure 2: Persistent behavioural tracking of noni odours in *D. sechellia*.
a, Schematic of the tethered fly behavioural assay. *ΔWBA*: left-right difference of standardised wing beat amplitudes (see **Methods** for details), TTL: Transistor–transistor logic.
b, Odour-tracking behaviour towards noni juice and control stimuli (H_2O) in wild-type *D. sechellia* (DSSC 14021-0248.07) and *D. melanogaster* (CS) flies. Left, time course of *ΔWBA* (mean ± SEM) where black bars indicate the timing of odour stimulation (ten 500 ms pulses with 500 ms intervals). Right, quantification in 1 s time windows immediately prior to stimulus onset ("pre") and thereafter corresponding to individual stimulus pulses ("1-10"). Mean ± SEM are shown (raw data are provided in the Source Data). Paired *t*-test *** $P < 0.001$; ** $P < 0.01$; * $P < 0.05$, otherwise $P > 0.05$. $n = 30$ animals each.
c, Odour-tracking behaviour towards noni juice in *D. sechellia Or* and *Ir* mutants. Paired *t*-test, *** $P < 0.001$; ** $P < 0.01$; * $P < 0.05$, otherwise $P > 0.05$. $n = 30$ animals each.
d, Left, example trajectories (black lines) in the x-y plane of *D. sechellia* (DSSC 14021-0248.07), *D. melanogaster* (a hybrid *Heisenberg-Canton-S* (*HCS*); our *CS* strain exhibited poor flight performance in this assay) and *D. sechellia Or22a*^{RFP} mutants flying in the presence of a noni plume (origin at the orange dot). Right, occupancy heat maps of trajectories that came at least once within 10 cm of the plume centreline for *D. melanogaster* ($n = 1346$ trajectories, 4 recording replicates, 60 flies), *D. sechellia* wild-type ($n = 835$ trajectories, 7 recording replicates, 105 flies) and *D. sechellia Or22a*^{RFP} mutants ($n = 509$ trajectories, 6 recording replicates, 90 flies).
e, Annotated view of the wild-type *D. sechellia* trajectories (from **d**) illustrating the data analyses performed in **f,g**. Based upon the trajectory distribution, we inferred that the noni juice plume sank by ~5 cm from the odour nozzle to the end of the tracking zone in the wind tunnel; this is likely due to the odour-laden air's higher water content (and so higher density) than the surrounding air. We therefore estimated the plume centre as a line connecting the nozzle and a point 5 cm lower in the z-axis at the end of the wind tunnel. Our results are qualitatively robust whether or not we account for plume sinking (**Extended Data Fig. 4d-f**).
f, Mean radial distance of the point cloud from the plume centreline for the trajectories in **d**. Data were binned into 5 cm y-z plane cross-sections starting 5 cm downwind from the plume origin, and restricted to 10 cm altitude above or below the estimated plume model. Non-parametric bootstrapped comparison of medians $P < 0.001$.
g, Kernel density of the course direction distribution of points within a 3 cm radius of the plume centreline (orange circle on cross-section in **e**), further parsed into the point cloud in the downwind or upwind halves of the wind tunnel (see **e**). Downwind half kernels: *D. melanogaster* (20,912 points from 511 unique trajectories), *D. sechellia* wild-type (15,414 points from 367 trajectories), *D. sechellia Or22a*^{RFP} (3,244 points from 164 unique trajectories). Upwind half kernels: *D. melanogaster* (80,594 points from 615 unique trajectories), *D. sechellia* wild-type (136,827 points from 501 unique trajectories), *D. sechellia Or22a*^{RFP} (40,560 points from 286 unique trajectories).

Figure 3: Behavioural significance of OSN number.
a, Optogenetic stimulation of Or22a OSNs in *D. melanogaster* (top) and *D. sechellia* (bottom). Left, expression of CsChrimson in the antenna detected by

expression of the Venus tag. Scale bar, 20 µm. Middle, single-sensillum recordings of Or22a OSNs in response to optogenetic stimulation of CsChrimson-expressing and control sensilla. The red line links the mean neuronal response at each light intensity, overlaid with individual data points. The black frame indicates the light intensity used for behavioural experiments. n = 5-10 sensilla (exact numbers are listed in **Extended Data Table 1**), unpaired Student's t-test, *** $P < 0.001$; * $P < 0.05$, otherwise $P > 0.05$. Right, behavioural responses of the same genotypes in response to red light stimulation (ten 500 ms pulses with 500 ms intervals, indicated by the red bars). Paired t-test, ** $P < 0.01$; * $P < 0.05$, otherwise $P > 0.05$. n = 29 (*D. melanogaster*) and 30 (*D. sechellia*) animals. Genotypes: *D. melanogaster w;UAS-CsChrimson-Venus/+* (control), *w;UAS-CsChrimson-Venus/Or22a-Gal4* (experimental), *D. sechellia w;;UAS-CsChrimson-Venus/+* (control), *w;Or22a^{Gal4}/+;UAS-CsChrimson-Venus/+* (experimental).

b, Behavioural responses of *D. sechellia* upon optogenetic stimulation of Or22a OSNs (top) and to noni odour stimulation (middle), in the same animals. Bottom, comparison of *ΔWBA* between light and odour responses. Paired t-test, *** $P < 0.001$, ** $P < 0.01$, * $P < 0.05$, otherwise $P > 0.05$. n = 27 animals each. Genotype as in **a**.

c, Sparse activation of *D. sechellia* Or22a OSNs. Left, expression of CsChrimson in an antenna of *D. sechellia* expressing *UAS-SPARC2-D-CsChrimson-Venus* in Or22a OSNs. Fluorescent labelling was sparser than in *UAS-CsChrimson-Venus* expressing animals but the dense packing of membrane-labelled neurons prevented quantification. Experiments in *D. melanogaster* (**Extended Data Fig. 6b**) and with the *UAS-SPARC2-D-TNT-HA* transgene (below) support expression in ~50% of Or22a OSNs with this SPARC version. Scale bar, 20 µm. Middle, single-sensillum recordings of Or22a OSNs in response to optogenetic stimulation. ab3 sensilla were first identified by stimulation with diagnostic odours (not shown); responses of CsChrimson-expressing neurons (experimental group) and non-expressing neurons (control, often from the same animal) are shown. n = 8-9 (exact numbers are listed in **Extended Data Table 1**), unpaired t-test, *** $P < 0.001$; * $P < 0.05$, otherwise $P > 0.05$. Right, *D. sechellia* behaviour upon optogenetic activation of about half of their Or22a expressing neurons. Paired t-test, *** $P < 0.001$; * $P < 0.05$; otherwise $P > 0.05$. n = 26 animals. Genotypes: *D. sechellia w;Or22a^{Gal4}/UAS-SPARC2-D-CsChrimson-Venus;;nSyb-ΦC31/+*.

d, Sparse inhibition of *D. sechellia* Or22a OSNs. Left, HA immunofluorescence in an antenna of *D. sechellia* (females) expressing *UAS-SPARC2-D-TNT-HA* in Or22a OSNs. Scale bar, 20 µm. Quantification of cell-labelling is shown below. Middle, *D. sechellia* odour-tracking behaviour towards noni juice of flies in effector control (top), driver control (middle), or in experimental animals with blocked synaptic transmission in approximately half of their Or22a neurons (bottom). Paired t-test, *** $P < 0.001$; ** $P < 0.01$; * $P < 0.05$; otherwise $P > 0.05$. n = 34 animals each. Genotypes: *D. sechellia w;UAS-SPARC2-D-TNT-HA-GeCO/+;;+/+* (effector control), *D. sechellia w;Or22a^{Gal4}/+;;nSyb-ΦC31/+* (driver control), *D. sechellia w;Or22a^{Gal4}/UAS-SPARC2-D-TNT-HA-GeCO;;nSyb-ΦC31/+* (experimental group).

Figure 4: Increased sensory and synaptic pooling in noni-sensing glomeruli.

a, Schematic of OSN-PN connectivity in the antennal lobe. Or22a OSNs (orange) and Or85b OSNs (blue) have cell bodies in the antenna and axons projecting to the DM2 and VM5d glomerulus, respectively. The soma of second-order PNs

(green) are located in three distinct clusters around the antennal lobe (ad, anterodorsal; l, lateral; v, ventral); these neurons synapse with OSNs (the majority constrained to a single glomerulus) and send axonal projections to higher olfactory centres. For clarity, LN are not illustrated (see text)

b, Transgenic labelling of PNs in the *D. sechellia* antennal lobe using the *VT033006-Gal4* or *VT033008-Gal4* drivers to express *UAS-GCaMP6f* (here used simply as a fluorescent reporter). Immunofluorescence on whole-mount brains was performed with antibodies against GFP (detecting GCaMP6f) and nc82 (labelling the synaptic protein Bruchpilot[86]). The VM5d glomerulus is demarcated by a white line in the *VT033008-Gal4* line. Scale bar, 25 µm.

c, Left, representative image of VM5d PNs labelled by photo-activatable GFP (PA-GFP) in *D. melanogaster* and *D. sechellia*. Genotypes: *D. melanogaster UAS-C3PA-GFP/+;UAS-C3PA-GFP/VT033008-Gal4* (for VM5d PNs) or *UAS-C3PA-GFP/+;UAS-C3PA-GFP/VT033006-Gal4* (for DM2 PNs); *D. sechellia UAS-C3PA-GFP/VT033008-Gal4* (for VM5d PNs) or *UAS-C3PA-GFP/VT033006-Gal4* (for DM2 PNs). Arrows indicate the PN cell bodies; faint background GFP signal in other soma are irrelevant neuron types. The antennal lobe (AL) is demarcated by a dashed line. Scale bar, 25 µm. Right, quantification of Or22a and Or85c/b PN numbers innervating the DM2 and VM5d glomeruli, respectively, by labelling with PA-GFP (using two different driver lines for VM5d PNs) in *D. sechellia* and *D. melanogaster*. Mann-Whitney *U*-test, NS, not significant. $P > 0.05$.

d, Visualisation of antennal lobe glomeruli by expression of the Dα7-GFP post-synaptic marker in PNs. Genotypes: *D. melanogaster w;;VT033006-Gal4/UAS-Dα7-GFP*; *D. sechellia w;VT033006-Gal4/+;UAS-Dα7-GFP/+*. Scale bar, 20 µm.

e, Quantification of the volumes of DM2, VM5d and a control glomerulus, DM6 (innervated by Or67a neurons) in *D. sechellia* and *D. melanogaster* (females). Wilcoxon signed-rank test. $^{**}P < 0.005$; $^{***}P < 0.001$.

f, Representative images of single dye-labelled VM5d PNs in *D. melanogaster* and *D. sechellia* Genotypes: *D. melanogaster w;VM5d-Gal4/UAS-GFP*, *D. sechellia w;VM5d-Gal4/UAS-myrGFP* (the GFP fluorescence is not shown). Scale bar, 5 µm. Right, quantification of VM5d PN dendrite surface area and volume. Student's *t*-test. $^{*}P < 0.05$.

g, Left, representative images of post-synaptic puncta in VM5d, DM2 and DM6 PNs labelled by Dα7-GFP in *D. melanogaster* and *D. sechellia* (genotypes as in **d**). Scale bar, 5 µm. Right, quantification of the number of post-synaptic puncta in these glomeruli. Wilcoxon signed-rank test. $^{**}P < 0.005$; $^{***}P < 0.001$.

Figure 5: Sustained representation of noni odour stimuli in PNs of *D. sechellia*.

a-d, Whole-cell patch clamp recording from VM5d PNs in *D. melanogaster* and *D. sechellia*; the glomerular circuit is schematised on the left. Genotypes as in **Fig. 4f**. **a**, Voltage trace of VM5d PNs in response to a pulse of *2*-heptanone. **b-d**, Comparison of input resistance (**b**), resting membrane potential (**c**), and spontaneous activity (**d**) between *D. melanogaster* and *D. sechellia*. Student's *t*-test. $^{**}P < 0.01$. n = 4-5.

e, Dose-response relationship of VM5d PN firing to *2*-heptanone. Quantification of spike frequency was performed in a 50 ms window covering the peak response. Student's *t*-test. $^{**}P < 0.01$, $^{*}P < 0.05$. n =2-5 animals (exact numbers and mean responses are listed in **Extended Data Table 1**). EC_{50} values [Log] are as follows: -7.46 (*Dmel*), -6.87 (*Dsec*).

f, VM5d PN spike frequency in response to 10^{-6} dilution of *2*-heptanone. Left, time course of spike frequency. Mean ± SEM are shown. Right, quantification of the decay magnitude (i.e. start (first 50 ms) - end (last 500 ms before odour offset)). Student's *t*-test. *$P < 0.05$. $n = 5$ animals each.

g-h, Dose-dependent, odour-evoked calcium responses in Or85b/VM5d (**g**) and Or22a/DM2 (**h**) OSN axon termini and PN dendrites in the antennal lobe of *D. melanogaster* and *D. sechellia*, reported as normalised GCaMP6f fluorescence changes. Plots are based on the data in **Extended Data Fig. 8**. EC_{50} values [Log] are as follows: Or85b OSNs: -6.50 (*Dmel*), -6.51 (*Dsec*); VM5d PNs: -7.82 (*Dmel*), -7.87 (*Dsec*); Or22a OSNs: -7.42 (*Dmel*), -8.23 (*Dsec*); DM2 PNs: -7.97 (*Dmel*), -9.61 (*Dsec*). Genotypes are as follows. OSN calcium imaging: *D. melanogaster UAS-GCaMP6f/Orco-Gal4*,*UAS-GCaMP6f*, *D. sechellia UAS-GCaMP6f/UAS-GCaMP6f;;+/DsecOrco^{Gal4}*. PN calcium imaging: *D. melanogaster UAS-GCaMP6f/+;+/VT033008-Gal4* (for VM5d PNs), *D. melanogaster UAS-GCaMP6f/+;+/VT033006-Gal4* (for DM2 PNs), *D. sechellia UAS-GCaMP6f/VT033008-Gal4* (for VM5d PNs), *UAS-GCaMP6f/VT033006-Gal4* (for DM2 PNs).

i, Responses of Or85b OSNs to pulsed odour stimuli (ten 200 ms pulses, each separated by 200 ms, as indicated by the black bars). For both species, left panels show the time course (mean ± SEM $\Delta F/F_0$) and right panels show the quantification of $\Delta F/F_0$ peak to the 1st and 10th stimulation. Paired *t*-test. ** $P < 0.01$, * $P < 0.05$. $n = 8$ animals each.

j-k, Pulsed odour responses of VM5d PNs (**j**) and DM2 PNs (**k**). Paired *t*-test, ** $P < 0.01$. $n = 8$ animals each.

l-m, Pulsed odour responses of VA2 (Or92a) and DM4 (Or59b) PNs (two control pathways where the number of cognate OSNs is conserved between species (**Fig. 1c**)). Paired *t*-test. *** $P < 0.001$; ** $P < 0.01$. $n = 6$ animals each. Dose response data for these neurons are provided in **Extended Data Fig. 11**. Genotypes are as for DM2 PN imaging in **h**.

Figure 6: Mechanisms of sustained PN responses in *D. sechellia*.

a, Odour pulse responses of VM5d PNs following application of a GABA antagonist. PN responses in normal AHL saline (left) or containing 100 µM picrotoxin + 50 µM CGP54626 (right). Paired *t*-test, *** $P < 0.001$, NS $P > 0.05$. $n = 8$ animals each. Genotypes are indicated in **Fig. 5g** legend.

b, Odour pulse responses of VM5d PNs following application of low doses (200 µM) of mecamylamine (nAChR antagonist) to weakly block cholinergic inputs. *D. melanogaster* and *D. sechellia* PN responses in normal AHL saline, mecamylamine and AHL saline wash-out. Paired *t*-test. *** $P < 0.001$, * $P < 0.05$, NS $P > 0.05$. $n = 7$ animals each.

c, Odour pulse responses of *D. sechellia* VM5d PNs in intact (top) and right antenna-ablated (bottom) animals, in which the OSN input is halved. Paired *t*-test, * $P < 0.05$, NS $P > 0.05$. $n = 7$ each.

d, Model illustrating the complementary effects of OSN sensitisation (due to receptor tuning) and reduced PN decay magnitude (putatively due to OSN population increases; see **Discussion**) on odour-evoked activity, which might synergise to promote sensitive and persistent long-range odour tracking toward the noni host fruit by *D. sechellia*, but not *D. melanogaster*.

Extended Data Figure Legends

Extended Data Figure 1: Investigation of potential mechanisms underlying ab3 sensilla expansion.

a, Quantification of *Or22a/(b)* RNA expressing OSNs in the antenna of six *D. sechellia*, *D. simulans* and *D. melanogaster* strains. For strain details see **Extended Data Table 2**. Wilcoxon signed-rank test, *P* values adjusted for multiple comparisons using the Benjamini and Hochberg method. Comparisons to *Dsec07* (genetic background of transgenic lines) are shown. NS, not significant ($P > 0.05$); $^{**}P < 0.01$; $^{***}P < 0.001$.

b, Top, immunofluorescence for GFP and RNA FISH for *Or85b* on whole-mount antennae from *D. melanogaster Or49b-GFP* animals. Arrowheads indicate paired neurons. Or85b neurons are housed in ab3 (with Or22a neurons) and ab6 sensilla (with Or49b neurons), but only the ab3 population is expanded in *D. sechellia* (**Fig. 1c**). Scale bar, 25 µm.

c, Comparison of the number of *Or22a* RNA-expressing OSNs in the antenna of *D. sechellia* raised on (left) and without (right) noni supplement. Scale bar, 25 µm. Quantification to the right. Wilcoxon rank-sum test. NS, $P > 0.05$.

d, Top left, schematic of the ab2 sensillum housing Or59b and Or85a neurons. Top right, RNA FISH for *Or59b* on whole-mount antennae from *D. melanogaster, D. simulans and D. sechellia* wild-type animals (females). Scale bar, 25 µm.

e, Top, schematic of developmental transitions from larval antennal disc to adult antenna. Schematic of the larval antennal disc, within which concentric arcs of sensory organ progenitors (SOPs) are specified, each of which gives rise to a sensillum. Different SOP types have a stereotyped developmental origin in a given arc (adapted from[28]). Arrows indicate the change in relative population size in *D. sechellia* compared to *D. melanogaster*. No obvious relationship between ab3 number increase and compensatory reduction in sensilla derived from SOPs in the same or neighbouring arcs is evident.

f, Representative pictures of the reciprocal hemizygosity test at the *Or22a/b* and *Or85c/b* loci using RNA FISH results shown in **Fig. 1d**. Schematics on top indicate expression from the respective alleles.

Extended Data Figure 2: Genetic analysis of OSN cell number expansion.

a, Left, schematics depicting the introduction of a nuclear-localised GFP reporter (GFPnls) at the *Or85b* locus of *D. sechellia* and *D. simulans* via CRISPR/Cas9 genome engineering. Right, GFP signal in antennae of *DsecOr85b*^{GFP} and *DsimOr85b*^{GFP} animals. Scale bar, 25 µm.

b, Immunofluorescence for GFP and *Or22a* RNA FISH on whole-mount antennae from *DsecOr85b*^{GFP} animals. Arrowheads indicate neighbouring neurons. Scale bar, 25 µm.

c, Introgression of chromosomal fragments marked with a transgenic RFP marker (dashed line) from *D. sechellia* into *D. simulans* spanning varying extents of the QTL peak on chromosome 3.

d, Left, quantification of GFP-expressing neurons in F2 backcrosses of the *D. sechellia* RFP transgenic line to *D. simulans Or85b*^{GFP} flies comparing RFP positive and negative siblings (females only). Right, quantification of GFP-expressing neurons in the five *D. sechellia* introgression lines depicted in **a**, comparing RFP positive and negative siblings. *n* are listed in the figure. Wilcoxon signed-rank test. NS, not significant ($P > 0.05$); $^{*}P < 0.05$; $^{***}P < 0.001$.

e, Left, location of the *lozenge* (*lz*) gene (dashed line) relative to the QTL peaks detected on the X chromosome. Right, schematics depicting the *lozenge* gene organisation and the structure of mutant alleles in both *D. sechellia* and *D. simulans*. The fluorescent marker was integrated into the first coding exon.
f, Comparison of antennal morphology in wild-type and *lz* mutant *D. sechellia* and *D. simulans*. In both species, loss of *lz* results in a lack of basiconic sensilla (white arrowheads) compared to wild-type, similar to *D. melanogaster lz* mutants[85]. Scale bar, 25 µm; inset scale bar, 5 µm.
g, Quantification of GFP-expressing neurons in $DsimlZ^{RFP}$ heterozygote mutant and wild-type siblings (females only). Wilcoxon signed-rank test. $^{**}P < 0.01$.
h, Quantification of GFP-expressing neurons in $DseclZ^{RFP}$ heterozygote mutant and wild-type siblings (females only). Wilcoxon signed-rank test. $^{***}P < 0.001$.
i, Quantification of GFP-expressing neurons in *trans*-heterozygote hybrid siblings (females only) carrying either a $DseclZ^{RFP}$ or $DsimlZ^{RFP}$ allele. Wilcoxon signed-rank test. NS, not significant ($P > 0.05$).
j, Quantification of Ir75b neurons in wild-type *D. sechellia* (DSSC 14021-0248.25) and *D. simulans* (DSSC 14021-0251.195) (mixed genders) and respective F2 progeny derived from backcrosses of F1 hybrid females to either parental strain (mixed genders). The black line indicates the mean cell number.
k, Logarithm of odds (LOD) score across all four chromosomes for loci impacting Ir75b neuron numbers based on phenotyping data shown in **j**. Dashed horizontal lines mark $P = 0.05$; non-dashed horizontal lines mark $P = 0.01$.

Extended Data Figure 3: Odour-tracking behaviour of wild-type strains.
a, Odour-tracking behaviour towards noni juice in other wild-type strains of *D. sechellia* and *D. melanogaster* (see **Extended Data Table 2**), plotted as in **Fig. 2b.** Paired *t*-test, *** $P < 0.001$; ** $P < 0.01$; * $P < 0.05$; otherwise $P > 0.05$. $n = 30$ (*DmelBK, DmelrHR, Dsec19, Dsec31*) or 27 (*DmelOR, Dsec28*) animals.
b, Odour-tracking behaviour towards apple cider vinegar in wild-type *D. sechellia* strains. Paired *t*-test, *** $P < 0.001$; ** $P < 0.01$; * $P < 0.05$; otherwise $P > 0.05$. $n = 30$ animals each.

Extended Data Figure 4: Odour tracking in a wind tunnel.
a, Array of 12 tracking cameras above the wind tunnel used for 3D tracking of flies in the presence of a noni plume.
b, Side view of wind tunnel system along with the acrylic port used to flux noni odour into the tunnel volume.
c, Comparison of mean trajectory ground speeds for the three genotypes studied.
d, Schematic of two plume models used to analyse data compared to the point cloud distribution of *D. sechellia* trajectories in the wind tunnel volume. A “straight” model (solid orange line) which is aligned in space with the odour port, or a “sloped” model (dashed orange line) for which the plume sinks by 5 cm from the odour port to the tunnel end.
e, Radial distance calculations comparing mean radial distance of points from the plume centreline considering either the sloped or straight plume model (left two plots). The same data is also shown without the restriction to limit this analysis to 10 cm above or below the plume’s altitude (right two plots).
f, Left, course direction distributions within a 3 cm radius of the plume centreline for either the sloped plume model (as in **Fig. 2g**) for the downwind and upwind

halves of the wind tunnel, up to 5 cm downwind from the plume origin. Right, the same analysis assuming a straight plume model.

Extended Data Figure 5: Additional conditions of optogenetic stimulation.
a, Optic fibre-mediated illumination of one antenna in the tethered fly. The photo was taken from below the apparatus.
b, Behavioural responses to optogenetic stimulation of Or22a/b OSNs in *D. melanogaster* using a *Gal4* knock-in line (see **Fig. 3a** for methodological details) Genotype: *D. melanogaster w;Or22a/b^{Gal4}/UAS-CsChrimson-Venus*. Left, time course of *ΔWBA*. Right, quantification within each phase. Paired *t*-test, $P > 0.05$.
c, Behavioural responses to optogenetic stimulation of effector control flies (*UAS-CsChrimson-Venus*) in *D. melanogaster* (left) and *D. sechellia* (right). Paired *t*-test, $P > 0.05$. Genotypes: *D. melanogaster w;+/UAS-CsChrimson-Venus, D. sechellia w;;;+/UAS-CsChrimson-Venus.*
d, Behavioural responses to optogenetic stimulation of Or22a OSNs in *D. sechellia* using CsChrimson by stimulating the left antenna induces leftward turning behaviour (resulting in reduced *ΔWBA* values compared to control flies). Paired *t*-test, ** $P < 0.01$; * $P < 0.05$; otherwise $P > 0.05$. Genotype as in **Fig. 3a**.

Extended Data Figure 6: SPARC2 allows genetic manipulation of a subset of Or22a OSNs.
a, Schematic illustrating the principle of SPARC2[35]. Top, *Φ*C31-mediated recombination leads to removal of a stop cassette flanked by attP sites. Co-expression of Gal4 in the same cell leads to transcriptional activation of a reporter gene. Middle, recombination with an alternative attP site does not lead to a functional read-out. Depending on the attP version present in the cassette, recombination efficiencies vary (D, dense; I, intermediate; S, sparse). Bottom, after recombination, a proportion of Gal4-expressing cells – in this study Or22a OSNs – will express the respective SPARC2 transgene.
b, Left, immunofluorescence for GFP on whole-mount antennae from animals expressing different *SPARC2-X-GFP* versions in Or22a neurons. Right, quantification of the number of Or22a OSNs labelled by SPARC2 versions in *D. melanogaster*. Genotypes: *D. melanogaster nSyb-ΦC31/+;Or22a^{Gal4}/UAS-SPARC2-X-GFP*. The SPARC2-D transgene labelled ~50% of Or22a OSNs (compare with **Fig. 1c**) and was therefore used to generate transgenic constructs in *D. sechellia*.
c, Optogenetic stimulation of Or22a OSNs in *D. sechellia* using a lower light intensity. Electrophysiological measurements confirm that this light intensity evokes a similar degree of OSN firing as in the SPARC2-D-CsChrimson experiment. Paired *t*-test. * $P < 0.05$; otherwise $P > 0.05$. Electrophysiological data are re-plotted from **Fig. 3a**.
d, Immunofluorescence for for HA and nc82 on a whole-mount brain of *D. sechellia Or22a^{Gal4}* transgenic flies expressing *UAS-SPARC2-D-TNT-HA-GeCO*, revealing selective strong expression in Or22a OSNs projecting to DM2. The white arrowheads point to a few cells (putative glia due to their apparent lack of processes) labelled in the central brain. Scale bar, 50 µm.

Extended Data Figure 7: Whole-cell patch clamp recordings from VM5d PNs.
a, Voltage trace (top) and peri-stimulus time histogram (PSTH, bottom) of VM5d PN responses to a dilution series of *2*-heptanone. Mean is shown for the voltage trace and mean ± SEM are shown for the PSTH. *n* = 2-5 animals.
b, Start and end responses of VM5d PN to various dilutions of *2*-heptanone. Quantification at the start (first 50 ms), end (last 500 ms before odour offset) and decay magnitude (start - end) spike frequencies are shown. Student's *t*-test. $*P < 0.05$. *n* = 2-5 animals (mean values and SEM for each concentration listed in **Extended Data Table 1**).

Extended Data Figure 8: Dose-response odour responses of OSNs and PNs in Or85b and Or22a pathways.
a-b, Representative odour-evoked calcium responses in the axon termini of Or85b OSNs (**a**) and dendrites of VM5d PNs (**b**) in *D. melanogaster* and *D. sechellia.* Far left, schematic of the OSN-PN populations under investigation; the population subject to imaging analysis in shown in a darker colour. Left, representative confocal images of the raw fluorescence of GaMP6f showing the plane used for imaging with glomerular labels; corresponding solvent and odour stimulus-induced fluorescent changes are also shown. Middle panels, time courses in response to solvents and two odour dilutions (mean ± SEM $\Delta F/F_0$, bars indicate the timing of stimulus). Right, quantifications of peak $\Delta F/F_0$ for a dilution series of each odour (Dunnett's test, control: solvent, *** $P < 0.001$; * $P < 0.01$; * $P < 0.05$; otherwise $P > 0.05$, *n* = 7 (*D. melanogaster* OSNs), 8 (*D. sechellia* OSNs), 7 (*D. melanogaster* PNs), 6 (*D. sechellia* PNs) animals. Genotypes are indicated in **Fig. 5g** legend.
c-d, Representative odour-evoked calcium responses in the axon termini of Or22a OSNs (**c**) and DM2 PNs (**d**) in *D. melanogaster* and *D. sechellia. n* = 10 animals each. Genotypes are indicated in **Fig. 5g** legend.
e, Calcium imaging of DM2 PNs following reintroduction of *DmelOr22a* or *DsecOr22a* in Or22a OSNs in *D. melanogaster* lacking endogenous receptor expression. Left, time courses of odour responses. Middle, quantifications of peak $\Delta F/F_0$ (Dunnett's test, control: solvent, *** $P < 0.001$; * $P < 0.01$; * $P < 0.05$; otherwise $P > 0.05$,). *n* = 7 animals each. Right, normalised GCaMP6f fluorescence changes. Genotypes: *D. melanogaster w*;*Or22a/b*^{Gal4}/*Or22a/b*^{Gal4};*UAS-DmelOr22a*,*VT033006-LexA*/*VT033006-LexA,LexAop-GCaMP6m* (*DmelOr22a* allele rescue), *w*;*Or22a/b*^{Gal4}/*Or22a/b*^{Gal4};*UAS-DsecOr22a*,*VT033006-LexA*/*VT033006-LexA,LexAop-GCaMP6m* (*DsecOr22a* allele rescue).

Extended Data Figure 9: Odour response reliability.
Odour response reliability of VM5d PNs. **a-b**, Calcium responses of VM5d PNs in response to repeated stimulation with *2*-heptanone (concentration (Log) indicated on the figure) in *D. melanogaster* (**a**) and *D. sechellia* (**b**). Left, quantification of peak $\Delta F/F_0$ from eight trials of stimulation. Dunnett's test, compared to control (Trial 1). NS ($P > 0.05$). *n* = 8 animals each. Right, time courses of responses in trial 1 and 8 shown as mean ± SEM $\Delta F/F_0$. The odour stimulus (1 s) is shown with a black bar. **c**, Quantification of mean, standard deviation and coefficient of variation of peak $\Delta F/F_0$ across the eight stimulation trials. Welch's *t*-test. NS ($P > 0.05$).

Extended Data Figure 10: *D. sechellia* VM5d PNs show persistent response to long odour stimulation

Calcium responses of Or85b/VM5d neurons in response to long odour stimulation of *D. melanogaster* Or85b OSNs (**a**), *D. melanogaster* VM5d PNs (**b**), *D. sechellia* OSNs (**c**), and *D. sechellia* PNs (**d**). Left, time courses of the odour response (mean ± SEM $\Delta F/F_0$). Bars indicate the timing of long odour stimulation (10 s). Right, maximum $\Delta F/F_0$ in the first and last 2.5 s time windows are compared. Paired *t*-test. ** $P < 0.01$; ** $P < 0.05$. $n = 7$ (OSNs) or 8 (PNs) animals for both species. Genotypes are indicated in the **Fig. 5g** legend.

Extended Data Figure 11: Odour response sensitivity in control glomeruli.

Odour-evoked dose-dependent calcium responses in control glomeruli of *D. melanogaster* VA2 (Or92a) PNs (**a**), *D. sechellia* VA2 PNs (**b**), *D. melanogaster* DM4 (Or59b) PNs (**c**), and *D. sechellia* DM4 PNs (**d**). Left, time courses in response to solvents and specific odour dilutions (mean ± SEM $\Delta F/F_0$, bars indicate the timing of stimuli). Right, quantifications of peak $\Delta F/F_0$ (Dunnett's test, control: solvent, *** $P < 0.001$; * $P < 0.01$; * $P < 0.05$; otherwise $P > 0.05$,). $n = 7$ each. The genotype for the VA2 and DM4 PN calcium imaging is the same as for DM2 PN imaging shown in **Fig. 5g**.

Extended Data Figure 12: Pharmacological manipulations of lateral inhibition.

a,b, Odour pulse responses of VM5d PNs following application of a $GABA_A$ (**a**, Picrotoxin) and $GABA_B$ (**b**, CGP54626) antagonist. PN responses in normal AHL saline (left) or containing 100 µM picrotoxin or 50 µM CGP54626 (middle). The ratio between 10th and 1st odour pulses are shown on the far right. Paired *t*-test. ** $P < 0.01$, * $P < 0.05$, NS $P > 0.05$. $n = 7$ animals each. Genotypes are indicated in **Fig. 5g** legend.

c, Raw GCaMP fluorescence intensity in VM5d PNs in *D. melanogaster* (left) and *D. sechellia* (right) following GABA antagonist application. Mean fluorescence before (4-5 s; as "Baseline") and during (5-9 s; as "Odour") the stimulus was quantified. Paired *t*-test, ** $P < 0.01$, * $P < 0.05$, NS $P > 0.05$. $n = 8$ animals each. Genotype as in **Fig. 5g**.

Extended Data Figure 13: Variation in neuron numbers within and across species.

a, Correlation between OSN number and synapse numbers across glomeruli from *D. melanogaster* OSN quantification[18] and connectome[37] data. OSN outputs were quantified separately for connections to PNs (left), LNs (middle), and OSNs (right). *r* and *p* values are calculated by Pearson's correlation analysis.

b, Variation in basiconic sensilla neuron numbers in the *D. melanogaster* species subgroup. Numbers of Or42b, Or59b and Or22a/(b) neurons (housed in ab1, ab2 and ab3 sensilla, respectively) based on RNA FISH on whole-mount antennae across the *D. melanogaster* species subgroup; Ma, million years ago (n = 7-14, females). For strain details see **Extended Data Table 2**.

Extended Data Tables

Extended Data Table 1: Spike counts for electrophysiological experiments.

Extended Data Table 2: Wild-type and transgenic lines used and generated in this study.

Extended Data Table 3: Oligonucleotides used to generate single sgRNA expression vectors and *in situ* probe templates.

Extended Data Table 4: Oligonucleotides used to generate multi-sgRNA expression vectors.

References

1 Catania, K. C. A comparison of the Eimer's organs of three North American moles: the hairy-tailed mole (*Parascalops breweri*), the star-nosed mole (*Condylura cristata*), and the eastern mole (*Scalopus aquaticus*). *J Comp Neurol* **354**, 150-160, (1995).

2 Zhao, Z. & McBride, C. S. Evolution of olfactory circuits in insects. *J. Comp. Physiol. A Neuroethol. Sens. Neural Behav. Physiol.* **206**, 353-367, (2020).

3 Kudo, K., Shiraishi, J., Nishimura, S., Bungo, T. & Tabata, S. The number of taste buds is related to bitter taste sensitivity in layer and broiler chickens. *Anim Sci J* **81**, 240-244, (2010).

4 Linz, J. *et al.* Host plant-driven sensory specialization in *Drosophila erecta*. *Proceedings. Biological sciences / The Royal Society* **280**, 20130626, (2013).

5 Peichl, L. Diversity of mammalian photoreceptor properties: adaptations to habitat and lifestyle? *Anat Rec A Discov Mol Cell Evol Biol* **287**, 1001-1012, (2005).

6 Meisami, E. A proposed relationship between increases in the number of olfactory receptor neurons, convergence ratio and sensitivity in the developing rat. *Brain research. Developmental brain research* **46**, 9-19, (1989).

7 Auer, T. O., Shahandeh, M. P. & Benton, R. *Drosophila sechellia*: A Genetic Model for Behavioral Evolution and Neuroecology. *Annu Rev Genet* **55**, 527-554, (2021).

8 Jones, C. D. The genetics of adaptation in *Drosophila sechellia*. *Genetica* **123**, 137-145, (2005).

9 Stensmyr, M. C. *Drosophila sechellia* as a model in chemosensory neuroecology. *Ann N Y Acad Sci* **1170**, 468-475, (2009).

10 Herculano-Houzel, S. Not all brains are made the same: new views on brain scaling in evolution. *Brain Behav Evol* **78**, 22-36, (2011).

11 Godfrey, R. K. & Gronenberg, W. Brain evolution in social insects: advocating for the comparative approach. *J. Comp. Physiol. A Neuroethol. Sens. Neural Behav. Physiol.* **205**, 13-32, (2019).

12 Williams, R. W. & Herrup, K. The control of neuron number. *Annu. Rev. Neurosci.* **11**, 423-453, (1988).

13 Roberts, R. J. V., Pop, S. & Prieto-Godino, L. L. Evolution of central neural circuits: state of the art and perspectives. *Nat Rev Neurosci* **23**, 725-743, (2022).

14 Arendt, D., Bertucci, P. Y., Achim, K. & Musser, J. M. Evolution of neuronal types and families. *Curr. Opin. Neurobiol.* **56**, 144-152, (2019).

15 Leal, W. S. Odorant reception in insects: roles of receptors, binding proteins, and degrading enzymes. *Annu. Rev. Entomol.* **58**, 373-391, (2013).

16 Hansson, B. S. & Stensmyr, M. C. Evolution of insect olfaction. *Neuron* **72**, 698-711, (2011).

17 Benton, R. *Drosophila* olfaction: past, present and future. *Proc Biol Sci* **289**, 20222054, (2022).

18 Grabe, V. *et al.* Elucidating the Neuronal Architecture of Olfactory Glomeruli in the *Drosophila* Antennal Lobe. *Cell Rep* **16**, 3401-3413, (2016).

19 Couto, A., Alenius, M. & Dickson, B. J. Molecular, anatomical, and functional organization of the *Drosophila* olfactory system. *Curr Biol* **15**, 1535-1547, (2005).
20 Barish, S. & Volkan, P. C. Mechanisms of olfactory receptor neuron specification in *Drosophila*. *Wiley interdisciplinary reviews. Developmental biology* **4**, 609-621, (2015).
21 Yan, H. *et al.* Evolution, developmental expression and function of odorant receptors in insects. *J Exp Biol* **223**, jeb208215, (2020).
22 Prieto-Godino, L. L. *et al.* Evolution of Acid-Sensing Olfactory Circuits in Drosophilids. *Neuron* **93**, 661-676, (2017).
23 Auer, T. O. *et al.* Olfactory receptor and circuit evolution promote host specialization. *Nature* **579**, 402-408, (2020).
24 Dekker, T., Ibba, I., Siju, K. P., Stensmyr, M. C. & Hansson, B. S. Olfactory shifts parallel superspecialism for toxic fruit in *Drosophila melanogaster* sibling, *D. sechellia*. *Curr Biol* **16**, 101-109, (2006).
25 Ibba, I., Angioy, A. M., Hansson, B. S. & Dekker, T. Macroglomeruli for fruit odors change blend preference in *Drosophila*. *Die Naturwissenschaften* **97**, 1059-1066, (2010).
26 Alvarez-Ocana, R. *et al.* Odor-regulated oviposition behavior in an ecological specialist. *Nat Commun* **14**, 3041, (2023).
27 Stensmyr, M. C., Dekker, T. & Hansson, B. S. Evolution of the olfactory code in the *Drosophila melanogaster* subgroup. *Proc Biol Sci* **270**, 2333-2340, (2003).
28 Chai, P. C., Cruchet, S., Wigger, L. & Benton, R. Sensory neuron lineage mapping and manipulation in the *Drosophila* olfactory system. *Nat Commun* **10**, 643, (2019).
29 Andolfatto, P. *et al.* Multiplexed shotgun genotyping for rapid and efficient genetic mapping. *Genome Research* **21**, 610-617, (2011).
30 Prieto-Godino, L. L., Schmidt, H. R. & Benton, R. Molecular reconstruction of recurrent evolutionary switching in olfactory receptor specificity. *Elife* **10**, e69732, (2021).
31 Badel, L., Ohta, K., Tsuchimoto, Y. & Kazama, H. Decoding of Context-Dependent Olfactory Behavior in *Drosophila*. *Neuron* **91**, 155-167, (2016).
32 Straw, A. D., Branson, K., Neumann, T. R. & Dickinson, M. H. Multi-camera real-time three-dimensional tracking of multiple flying animals. *J R Soc Interface* **8**, 395-409, (2011).
33 van Breugel, F. & Dickinson, M. H. Plume-tracking behavior of flying *Drosophila* emerges from a set of distinct sensory-motor reflexes. *Curr Biol* **24**, 274-286, (2014).
34 Gaudry, Q., Hong, E. J., Kain, J., de Bivort, B. L. & Wilson, R. I. Asymmetric neurotransmitter release enables rapid odour lateralization in *Drosophila*. *Nature* **493**, 424-428, (2013).
35 Isaacman-Beck, J. *et al.* SPARC enables genetic manipulation of precise proportions of cells. *Nat. Neurosci.* **23**, 1168-1175, (2020).
36 Pan, J. W. *et al.* Patterns of transcriptional parallelism and variation in the developing olfactory system of *Drosophila* species. *Sci Rep* **7**, 8804, (2017).
37 Schlegel, P. *et al.* Information flow, cell types and stereotypy in a full olfactory connectome. *Elife* **10**, e66018, (2021).
38 Mosca, T. J. & Luo, L. Synaptic organization of the antennal lobe and its regulation by the Teneurins. *Elife* **3**, e03726, (2014).

39 Tirian, L. & Dickson, B. J. The VT GAL4, LexA, and split-GAL4 driver line collections for targeted expression in the *Drosophila* nervous system. *bioRxiv*, (2017).
40 Elkahlah, N. A., Rogow, J. A., Ahmed, M. & Clowney, E. J. Presynaptic developmental plasticity allows robust sparse wiring of the *Drosophila* mushroom body. *Elife* **9**, e52278, (2020).
41 Ellis, K. E. *et al.* Evolution of connectivity architecture in the *Drosophila* mushroom body. *bioRxiv*, doi:10.1101/2023.1102.1110.528036, (2023).
42 Mosca, T. J., Luginbuhl, D. J., Wang, I. E. & Luo, L. Presynaptic LRP4 promotes synapse number and function of excitatory CNS neurons. *Elife* **6**, e27347, (2017).
43 Leiss, F. *et al.* Characterization of dendritic spines in the *Drosophila* central nervous system. *Dev Neurobiol* **69**, 221-234, (2009).
44 Li, H. *et al.* Single-Cell Transcriptomes Reveal Diverse Regulatory Strategies for Olfactory Receptor Expression and Axon Targeting. *Curr Biol* **30**, 1189-1198 e1185, (2020).
45 Serences, J. T. Mechanisms of selective attention: response enhancement, noise reduction, and efficient pooling of sensory responses. *Neuron* **72**, 685-687, (2011).
46 Bhandawat, V., Olsen, S. R., Gouwens, N. W., Schlief, M. L. & Wilson, R. I. Sensory processing in the *Drosophila* antennal lobe increases reliability and separability of ensemble odor representations. *Nat. Neurosci.* **10**, 1474-1482, (2007).
47 Jeanne, J. M. & Wilson, R. I. Convergence, Divergence, and Reconvergence in a Feedforward Network Improves Neural Speed and Accuracy. *Neuron* **88**, 1014-1026, (2015).
48 Kazama, H. & Wilson, R. I. Homeostatic matching and nonlinear amplification at identified central synapses. *Neuron* **58**, 401-413, (2008).
49 Wilson, R. I. & Laurent, G. Role of GABAergic inhibition in shaping odor-evoked spatiotemporal patterns in the *Drosophila* antennal lobe. *J Neurosci* **25**, 9069-9079, (2005).
50 Liu, W. W. & Wilson, R. I. Glutamate is an inhibitory neurotransmitter in the *Drosophila* olfactory system. *Proceedings of the National Academy of Sciences of the United States of America* **110**, 10294-10299, (2013).
51 Olsen, S. R., Bhandawat, V. & Wilson, R. I. Divisive normalization in olfactory population codes. *Neuron* **66**, 287-299, (2010).
52 Wilson, R. I. Early olfactory processing in *Drosophila*: mechanisms and principles. *Annual review of neuroscience* **36**, 217-241, (2013).
53 Huang, J., Zhang, W., Qiao, W., Hu, A. & Wang, Z. Functional connectivity and selective odor responses of excitatory local interneurons in *Drosophila* antennal lobe. *Neuron* **67**, 1021-1033, (2010).
54 Tobin, W. F., Wilson, R. I. & Lee, W. A. Wiring variations that enable and constrain neural computation in a sensory microcircuit. *Elife* **6**, e24838, (2017).
55 Nagel, K. I., Hong, E. J. & Wilson, R. I. Synaptic and circuit mechanisms promoting broadband transmission of olfactory stimulus dynamics. *Nat. Neurosci.* **18**, 56-65, (2015).
56 Chou, Y. H. *et al.* Diversity and wiring variability of olfactory local interneurons in the *Drosophila* antennal lobe. *Nat. Neurosci.* **13**, 439-449, (2010).

57 Lee, D. & Benton, R. Comparative single-cell transcriptomic atlases reveal conserved and divergent features of drosophilid central brains. *bioRxiv*, doi:10.1101/2023.1111.1122.568274, (2023).
58 Turner, G. C., Bazhenov, M. & Laurent, G. Olfactory representations by *Drosophila* mushroom body neurons. *J Neurophysiol* **99**, 734-746, (2008).
59 Aso, Y. *et al.* Mushroom body output neurons encode valence and guide memory-based action selection in *Drosophila*. *Elife* **3**, e04580, (2014).
60 O'Mahony, M. Sensory Adaptation. *Journal of Sensory Studies* **1**, 237-258, (1986).
61 Keesey, I. W. *et al.* Functional olfactory evolution in *Drosophila suzukii* and the subgenus *Sophophora*. *iScience* **25**, 104212, (2022).
62 de Bruyne, M., Smart, R., Zammit, E. & Warr, C. G. Functional and molecular evolution of olfactory neurons and receptors for aliphatic esters across the *Drosophila* genus. *J. Comp. Physiol. A Neuroethol. Sens. Neural Behav. Physiol.* **196**, 97-109, (2010).
63 Backhaus, B., Sulkowski, E. & Schlote, F. W. A semi-synthetic general-purpose medium for *D. melanogaster*. *Drosophila Information Service* **60**, 210-212, (1984).
64 Port, F., Chen, H. M., Lee, T. & Bullock, S. L. Optimized CRISPR/Cas tools for efficient germline and somatic genome engineering in *Drosophila*. *Proceedings of the National Academy of Sciences of the United States of America* **111**, E2967-2976, (2014).
65 Port, F. & Bullock, S. L. Augmenting CRISPR applications in *Drosophila* with tRNA-flanked sgRNAs. *Nat Methods* **13**, 852-854, (2016).
66 Gratz, S. J. *et al.* Highly specific and efficient CRISPR/Cas9-catalyzed homology-directed repair in *Drosophila*. *Genetics* **196**, 961-971, (2014).
67 Talay, M. *et al.* Transsynaptic Mapping of Second-Order Taste Neurons in Flies by *trans*-Tango. *Neuron* **96**, 783-795 e784, (2017).
68 Klapoetke, N. C. *et al.* Independent optical excitation of distinct neural populations. *Nat Methods* **11**, 338-346, (2014).
69 Horn, C. & Wimmer, E. A. A versatile vector set for animal transgenesis. *Dev. Genes Evol.* **210**, 630-637, (2000).
70 Stern, D. L. Tagmentation-Based Mapping (TagMap) of Mobile DNA Genomic Insertion Sites. *bioRxiv*, 037762, (2017).
71 Arnoult, L. *et al.* Emergence and diversification of fly pigmentation through evolution of a gene regulatory module. *Science* **339**, 1423-1426, (2013).
72 Stern, D. L. *et al.* Genetic and Transgenic Reagents for *Drosophila simulans*, *D. mauritiana*, *D. yakuba, D. santomea* and *D. virilis*. *G3 (Bethesda)* **7**, 1339-1347, (2017).
73 Gratz, S. J., Wildonger, J., Harrison, M. M. & O'Connor-Giles, K. M. CRISPR/Cas9-mediated genome engineering and the promise of designer flies on demand. *Fly* **7**, (2013).
74 Gohl, D. M. *et al.* A versatile in vivo system for directed dissection of gene expression patterns. *Nature methods* **8**, 231-237, (2011).
75 Saina, M. & Benton, R. Visualizing olfactory receptor expression and localization in *Drosophila*. *Methods in Molecular Biology* **1003**, 211-228, (2013).
76 Silbering, A. F. *et al.* Complementary Function and Integrated Wiring of the Evolutionarily Distinct *Drosophila* Olfactory Subsystems. *The Journal of Neuroscience* **31**, 13357-13375, (2011).

77 Auer, T. O., Alvarez-Ocana, R., Cruchet, S., Benton, R. & Arguello, J. R. Copy number changes in co-expressed odorant receptor genes enable selection for sensory differences in drosophilid species. *Nature ecology & evolution* **6**, 1343-1353, (2022).

78 Vosshall, L. B., Wong, A. M. & Axel, R. An olfactory sensory map in the fly brain. *Cell* **102**, 147-159, (2000).

79 Sanchez-Alcaniz, J. A., Zappia, G., Marion-Poll, F. & Benton, R. A mechanosensory receptor required for food texture detection in *Drosophila*. *Nat Commun* **8**, 14192, (2017).

80 Schindelin, J. *et al.* Fiji: an open-source platform for biological-image analysis. *Nat Methods* **9**, 676-682, (2012).

81 Picelli, S. *et al.* Tn5 transposase and tagmentation procedures for massively scaled sequencing projects. *Genome Res* **24**, 2033-2040, (2014).

82 Silbering, A. F., Bell, R., Galizia, C. G. & Benton, R. Calcium imaging of odor-evoked responses in the *Drosophila* antennal lobe. *Journal of Vis Exp*, doi: 10.3791/2976, (2012).

83 Thevenaz, P., Ruttimann, U. E. & Unser, M. A pyramid approach to subpixel registration based on intensity. *IEEE Trans Image Process* **7**, 27-41, (1998).

84 Byk, T., Bar-Yaacov, M., Doza, Y. N., Minke, B. & Selinger, Z. Regulatory arrestin cycle secures the fidelity and maintenance of the fly photoreceptor cell. *Proceedings of the National Academy of Sciences of the United States of America* **90**, 1907-1911, (1993).

85 Gupta, B. P., Flores, G. V., Banerjee, U. & Rodrigues, V. Patterning an epidermal field: *Drosophila* lozenge, a member of the AML-1/Runt family of transcription factors, specifies olfactory sense organ type in a dose-dependent manner. *Dev. Biol.* **203**, 400-411, (1998).

86 Wagh, D. A. *et al.* Bruchpilot, a protein with homology to ELKS/CAST, is required for structural integrity and function of synaptic active zones in *Drosophila*. *Neuron* **49**, 833-844, (2006).

Figure 1

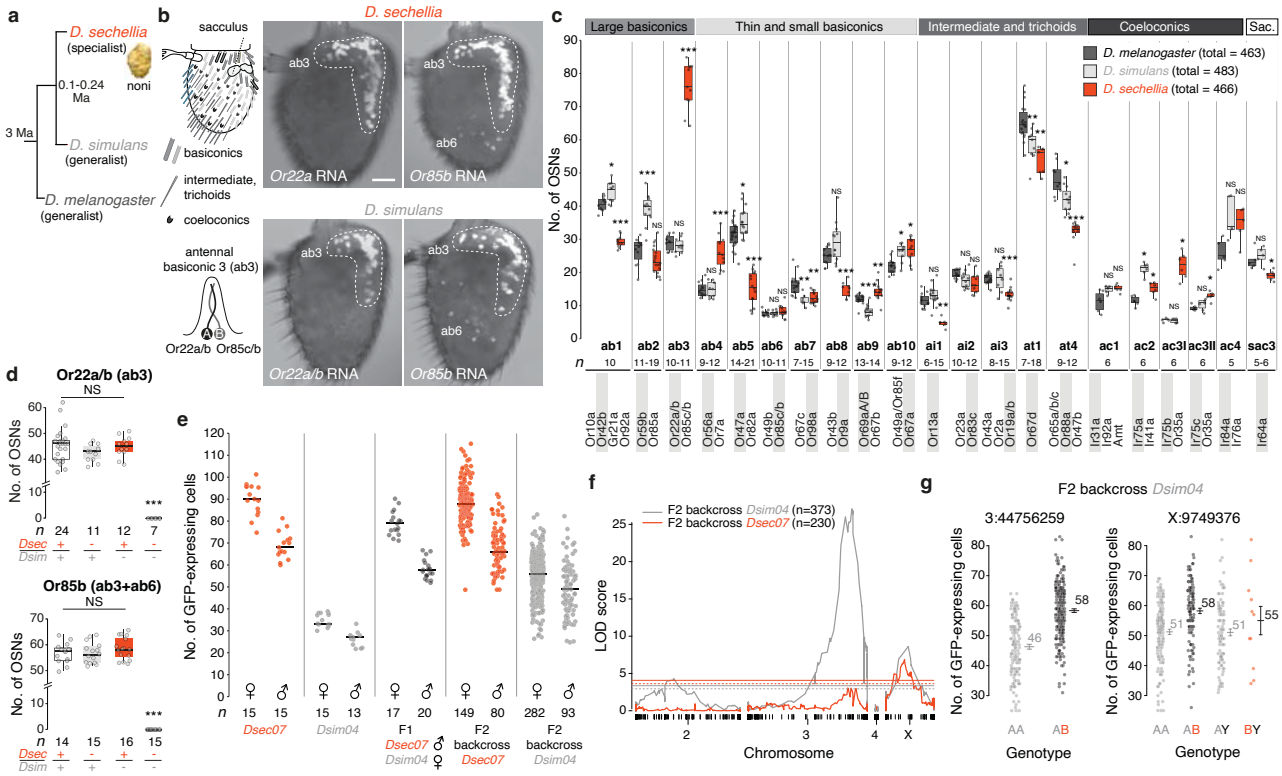
a
D. sechellia
(specialist)
noni
0.1-0.24 Ma
3 Ma
D. simulans
(generalist)
D. melanogaster
(generalist)
b
sacculus
basiconics
intermediate, trichoids
coeloconics
antennal basiconic 3 (ab3)
Or22a/b Or85c/b
D. sechellia
ab3
ab6
Or22a RNA
Or85b RNA
D. simulans
Or22a/b RNA
Or85b RNA
c
Large basiconics
Thin and small basiconics
Intermediate and trichoids
Coeloconics
Sac.
D. melanogaster (total = 463)
D. simulans (total = 483)
D. sechellia (total = 466)
No. of OSNs
ab1 ab2 ab3 ab4 ab5 ab6 ab7 ab8 ab9 ab10 ai1 ai2 ai3 at1 at4 ac1 ac2 ac3I ac3II ac4 sac3
n 10 11-19 10-11 9-12 14-21 10-11 7-15 9-12 13-14 9-12 6-15 10-12 8-15 7-18 9-12 6 6 6 6 5 5-6
Or10a Or42b Gr21a Or92a Or59b Or85a Or22a/b Or85c/b Or56a Or7a Or47a Or82a Or49b Or85c/b Or67c Or98a Or43b Or9a Or69aA/B Or67b Or49a/Or85f Or67a Or13a Or23a Or63c Or43a Or2a Or19a/b Or67d Or65a/b/c Or88a Or47b Ir31a Ir92a Amt Ir75a Ir41a Ir75b Or35a Ir75c Or35a Ir84a Ir76a Ir64a
d
Or22a/b (ab3)
NS
No. of OSNs
n 24 11 12 7
Dsec + - + -
Dsim + + - -
Or85b (ab3+ab6)
NS
No. of OSNs
n 14 15 16 15
Dsec + - + -
Dsim + + - -
e
No. of GFP-expressing cells
n 15 15 15 13 17 20 149 80 282 93
Dsec07 Dsim04 F1 Dsec07 ♂ Dsim04 ♀ F2 backcross Dsec07 F2 backcross Dsim04
f
F2 backcross Dsim04 (n=373)
F2 backcross Dsec07 (n=230)
LOD score
Chromosome
g
F2 backcross Dsim04
3:44756259
X:9749376
No. of GFP-expressing cells
Genotype
AA AB AY BY

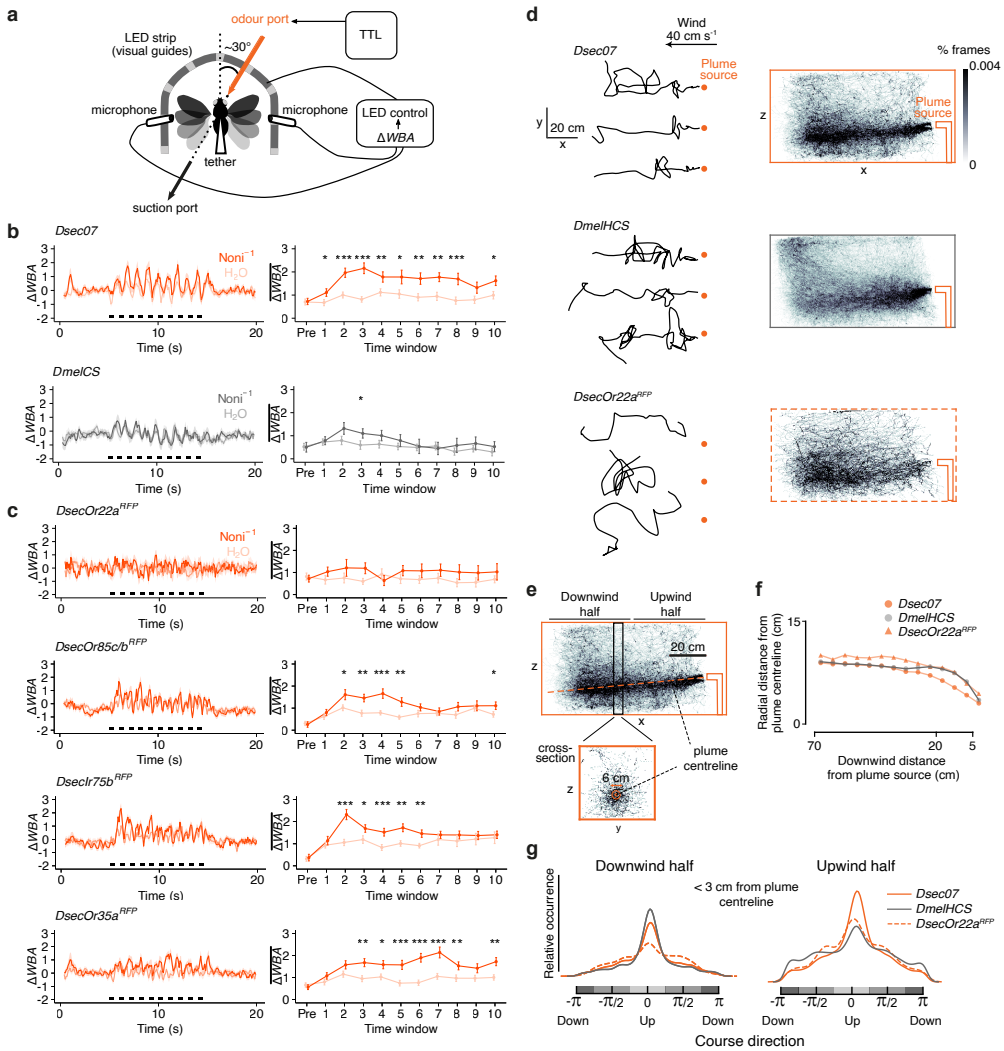
a
odour port
TTL
LED strip
(visual guides)
~30°
microphone
microphone
LED control
ΔWBA
tether
suction port
b
Dsec07
Noni⁻¹
H₂O
ΔWBA
Time (s)
Time window
DmelCS
c
DsecOr22a^RFP
DsecOr85c/b^RFP
DseclR75b^RFP
DsecOr35a^RFP
d
Wind
40 cm s⁻¹
Dsec07
Plume source
% frames
0.004
0
20 cm
DmelHCS
DsecOr22a^RFP
e
Downwind half
Upwind half
20 cm
cross-section
6 cm
plume centreline
f
Dsec07
DmelHCS
DsecOr22a^RFP
Radial distance from plume centreline (cm)
Downwind distance from plume source (cm)
g
Downwind half
Upwind half
< 3 cm from plume centreline
Relative occurrence
Course direction
Down
Up
Down

Figure 3

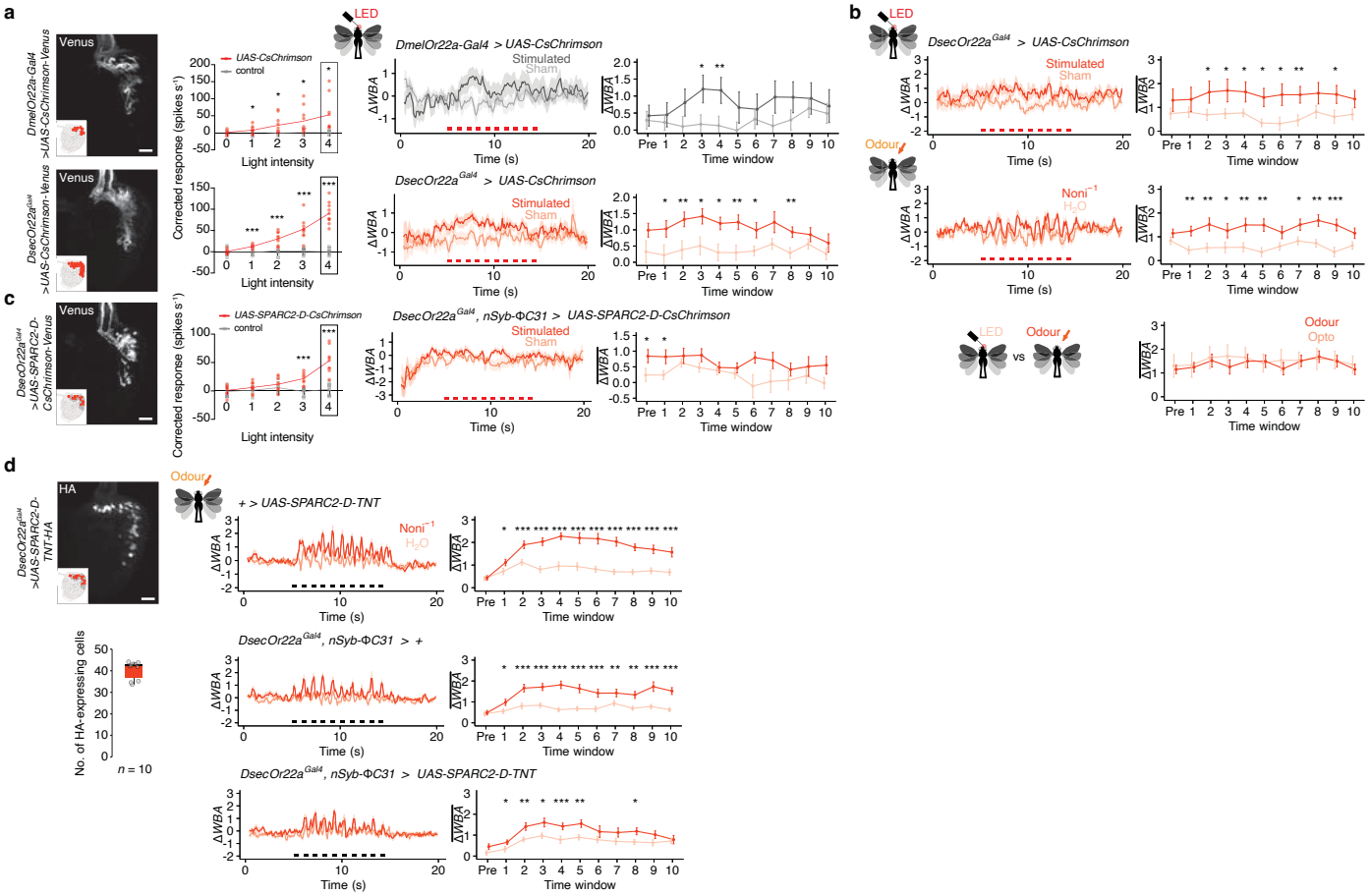
a
b
c
d
LED
Odour
Venus
HA
DmelOr22a-Gal4 >UAS-CsChrimson-Venus
DsecOr22a^Gal4 >UAS-CsChrimson-Venus
DsecOr22a^Gal4 >UAS-SPARC2-D-CsChrimson-Venus
DsecOr22a^Gal4 >UAS-SPARC2-D-TNT-HA
UAS-CsChrimson
control
UAS-SPARC2-D-CsChrimson
Corrected response (spikes s⁻¹)
Light intensity
DmelOr22a-Gal4 > UAS-CsChrimson
DsecOr22a^Gal4 > UAS-CsChrimson
DsecOr22a^Gal4, nSyb-ΦC31 > UAS-SPARC2-D-CsChrimson
Stimulated
Sham
ΔWBA
Time (s)
Time window
Pre
Noni⁻¹
H₂O
Odour
Opto
vs
+ > UAS-SPARC2-D-TNT
DsecOr22a^Gal4, nSyb-ΦC31 > +
DsecOr22a^Gal4, nSyb-ΦC31 > UAS-SPARC2-D-TNT
No. of HA-expressing cells
n = 10

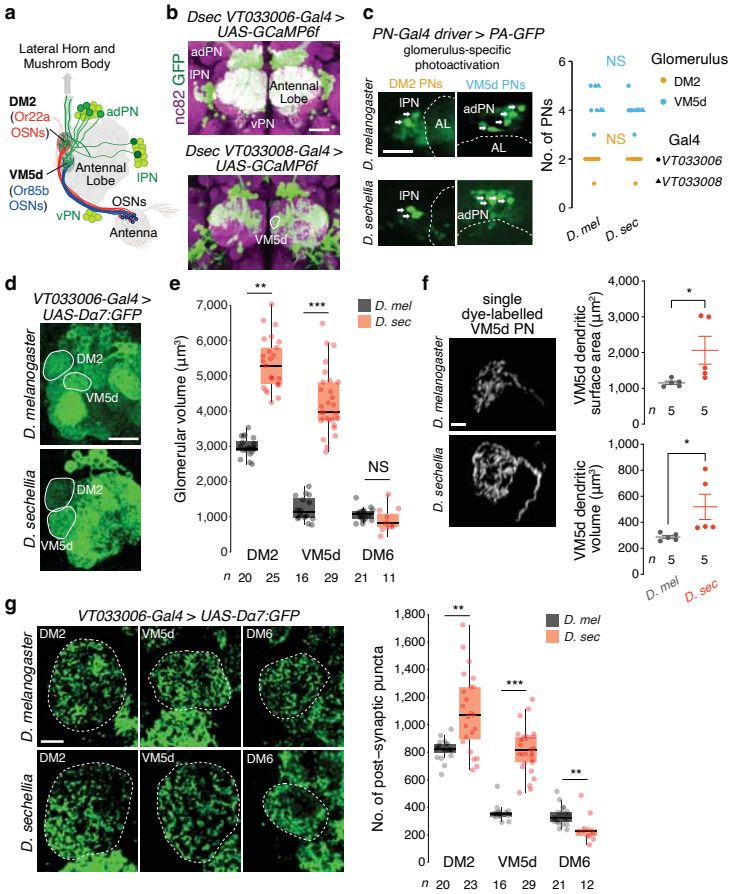
a
Lateral Horn and Mushrom Body
DM2 (Or22a OSNs)
adPN
VM5d (Or85b OSNs)
Antennal Lobe
IPN
OSNs
vPN
Antenna
b
Dsec VT033006-Gal4 > UAS-GCaMP6f
nc82 GFP
adPN
IPN
Antennal Lobe
vPN
Dsec VT033008-Gal4 > UAS-GCaMP6f
VM5d
c
PN-Gal4 driver > PA-GFP
glomerulus-specific photoactivation
DM2 PNs
VM5d PNs
D. melanogaster
D. sechellia
IPN
AL
adPN
No. of PNs
NS
Glomerulus
DM2
VM5d
Gal4
VT033006
VT033008
D. mel
D. sec
d
VT033006-Gal4 > UAS-Dα7:GFP
D. melanogaster
D. sechellia
DM2
VM5d
e
Glomerular volume (μm³)
D. mel
D. sec
**
***
NS
DM2
VM5d
DM6
n 20 25 16 29 21 11
f
single dye-labelled VM5d PN
D. melanogaster
D. sechellia
VM5d dendritic surface area (μm²)
VM5d dendritic volume (μm³)
*
n 5 5
D. mel
D. sec
g
VT033006-Gal4 > UAS-Dα7:GFP
D. melanogaster
D. sechellia
DM2
VM5d
DM6
No. of post-synaptic puncta
D. mel
D. sec
**
***
**
DM2
VM5d
DM6
n 20 23 16 29 21 12

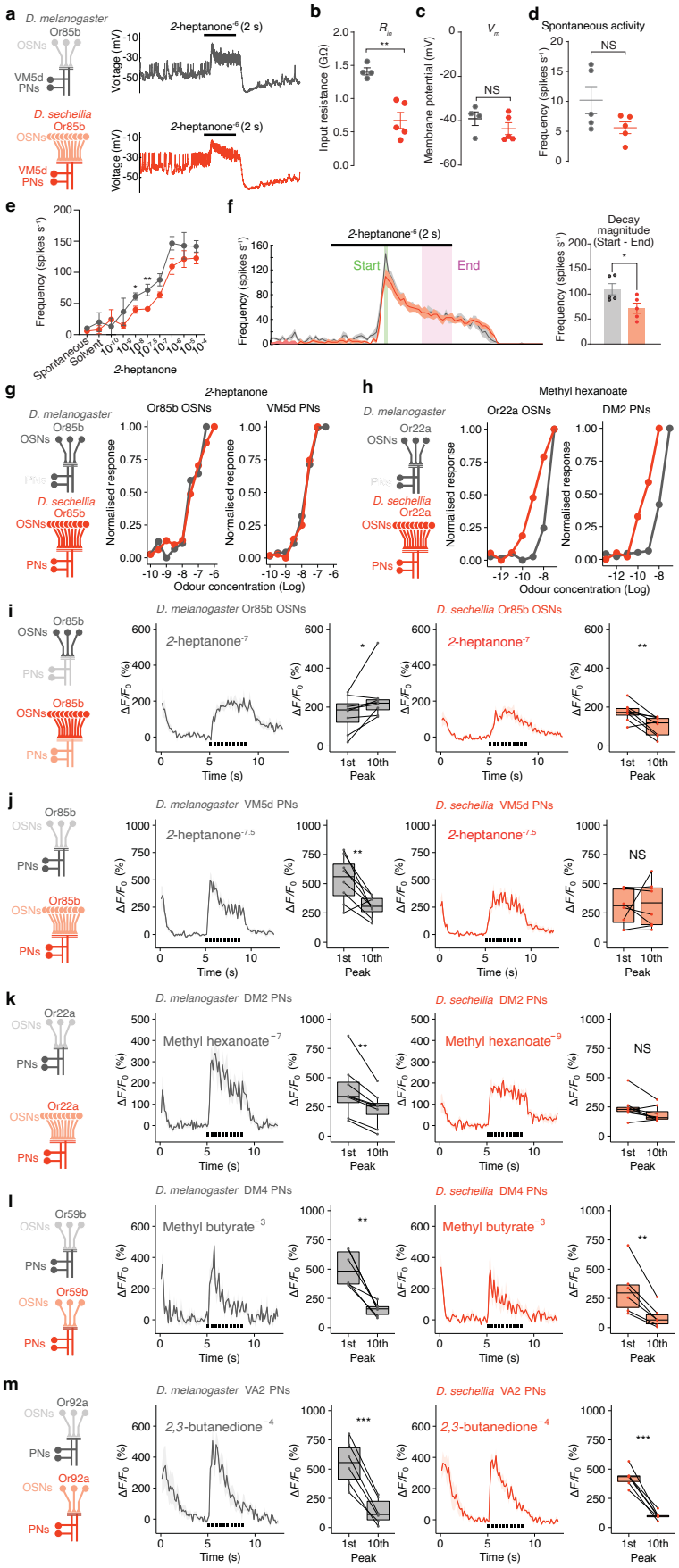
a
D. melanogaster
Or85b
OSNs
VM5d
PNs
D. sechellia
Or85b
OSNs
VM5d
PNs
2-heptanone-6 (2 s)
Voltage (mV)
b
Input resistance (GΩ)
c
Membrane potential (mV)
d
Spontaneous activity
Frequency (spikes s-1)
NS
e
Frequency (spikes s-1)
Spontaneous
Solvent
2-heptanone
f
2-heptanone-6 (2 s)
Start
End
Decay magnitude (Start - End)
g
2-heptanone
Or85b OSNs
VM5d PNs
Normalised response
Odour concentration (Log)
h
Methyl hexanoate
Or22a OSNs
DM2 PNs
i
D. melanogaster Or85b OSNs
D. sechellia Or85b OSNs
2-heptanone-7
ΔF/F0 (%)
Time (s)
Peak
1st
10th
j
D. melanogaster VM5d PNs
D. sechellia VM5d PNs
2-heptanone-7.5
k
D. melanogaster DM2 PNs
D. sechellia DM2 PNs
Methyl hexanoate-7
Methyl hexanoate-9
l
D. melanogaster DM4 PNs
D. sechellia DM4 PNs
Methyl butyrate-3
m
D. melanogaster VA2 PNs
D. sechellia VA2 PNs
2,3-butanedione-4

Figure 6

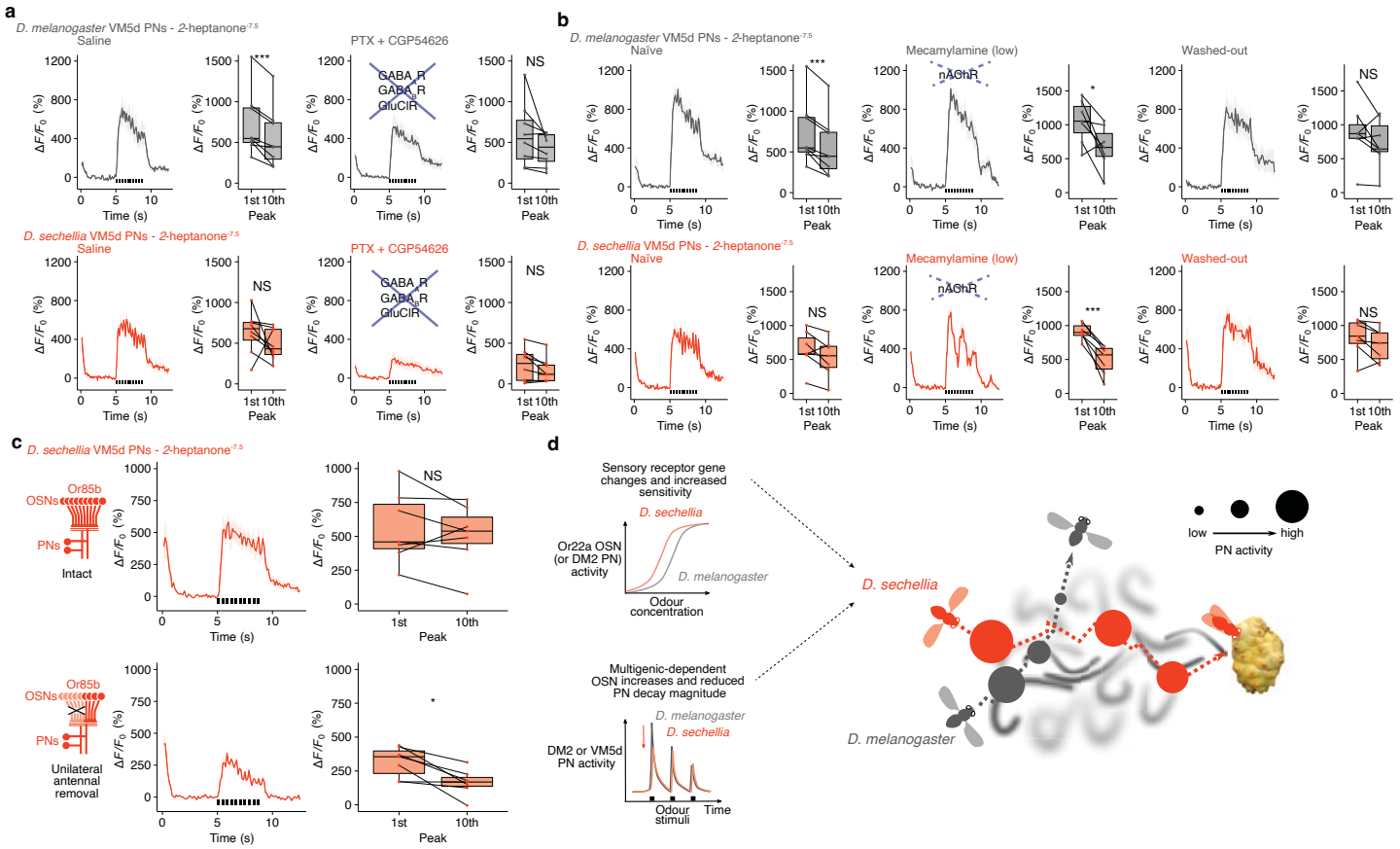
a
D. melanogaster VM5d PNs - 2-heptanone-7.5
Saline
PTX + CGP54626
GABA_R
GABA_R
GluClR
D. sechellia VM5d PNs - 2-heptanone-7.5
Saline
PTX + CGP54626
b
D. melanogaster VM5d PNs - 2-heptanone-7.5
Naïve
Mecamylamine (low)
nAChR
Washed-out
D. sechellia VM5d PNs - 2-heptanone-7.5
Naïve
Mecamylamine (low)
nAChR
Washed-out
ΔF/F0 (%)
Time (s)
Peak
1st
10th
NS
c
D. sechellia VM5d PNs - 2-heptanone-7.5
Or85b
OSNs
PNs
Intact
Unilateral antennal removal
d
Sensory receptor gene changes and increased sensitivity
D. sechellia
Or22a OSN (or DM2 PN) activity
D. melanogaster
Odour concentration
Multigenic-dependent OSN increases and reduced PN decay magnitude
DM2 or VM5d PN activity
Odour stimuli
Time
low
high
PN activity
D. sechellia
D. melanogaster